

Myostatin as a regulator of fiber size

Michal Solecki

A Thesis

in

The Department

of

Exercise Science

Presented in Partial Fulfillment of the Requirements
for the Degree of Master of Science (Exercise Science) at
Concordia University
Montreal, Quebec, Canada

August 2010

© Michal Solecki, 2010



Library and Archives
Canada

Published Heritage
Branch

395 Wellington Street
Ottawa ON K1A 0N4
Canada

Bibliothèque et
Archives Canada

Direction du
Patrimoine de l'édition

395, rue Wellington
Ottawa ON K1A 0N4
Canada

Your file *Votre référence*
ISBN: 978-0-494-71078-4
Our file *Notre référence*
ISBN: 978-0-494-71078-4

NOTICE:

The author has granted a non-exclusive license allowing Library and Archives Canada to reproduce, publish, archive, preserve, conserve, communicate to the public by telecommunication or on the Internet, loan, distribute and sell theses worldwide, for commercial or non-commercial purposes, in microform, paper, electronic and/or any other formats.

The author retains copyright ownership and moral rights in this thesis. Neither the thesis nor substantial extracts from it may be printed or otherwise reproduced without the author's permission.

In compliance with the Canadian Privacy Act some supporting forms may have been removed from this thesis.

While these forms may be included in the document page count, their removal does not represent any loss of content from the thesis.

AVIS:

L'auteur a accordé une licence non exclusive permettant à la Bibliothèque et Archives Canada de reproduire, publier, archiver, sauvegarder, conserver, transmettre au public par télécommunication ou par l'Internet, prêter, distribuer et vendre des thèses partout dans le monde, à des fins commerciales ou autres, sur support microforme, papier, électronique et/ou autres formats.

L'auteur conserve la propriété du droit d'auteur et des droits moraux qui protègent cette thèse. Ni la thèse ni des extraits substantiels de celle-ci ne doivent être imprimés ou autrement reproduits sans son autorisation.

Conformément à la loi canadienne sur la protection de la vie privée, quelques formulaires secondaires ont été enlevés de cette thèse.

Bien que ces formulaires aient inclus dans la pagination, il n'y aura aucun contenu manquant.


Canada

Abstract

Myostatin as a regulator of fiber size

Michal Solecki

Myostatin is an important negative regulator of muscle mass. Disruption of the myostatin gene leads to dramatic increases of skeletal muscle mass. Skeletal muscle is highly plastic and adapts in response to changes in workload, activity and pathological conditions. In this thesis, I set out to investigate the underlying mechanisms involved in growth in the absence of myostatin. We used the myostatin knockout model in combination with synergist ablation or denervation to study growth and atrophy.

During growth induced by functional overload, skeletal muscles increase their mass, midbelly and fiber cross-sectional area (CSA), and protein synthesis. The rapid growth also induces the activation and proliferation of satellite cells. In skeletal muscle, functional overload in myostatin knockout mice led to reduced growth in muscle mass and fiber size and a blunted switch of muscle fibers metabolic profile to a slower phenotype compared to their wildtype counterpart. Additionally, the distal portion of the plantaris was a region of major remodeling in both groups. Denervation through sciatic nerve section is an effective method to induce muscle atrophy. Following denervation, a rapid loss in muscle mass and fiber size occurs. Absence of myostatin did not prevent muscle mass and CSA loss in response to denervation. Moreover, no changes in the expression of MyHC isoforms were found.

In conclusion, myostatin is not the only regulator skeletal muscle mass. In its absence, alternative strategies are employed to reach a different outcome of growth and no protection from muscle atrophy was observed suggesting other mechanisms at play.

Acknowledgements

I would like to thank the following people:

Dr. Robin N. Michel: First, thank you for seeking out my potential to do great work. For the support and the great experience that I was able to achieve through this work.

My labmates (Mathieu, Ewa, Patrick, Manal and Moe): It was not easy but you have been really helpful over the years.

To my supervisory committee: For the great help and comments provided throughout my progress especially in those final days.

Mylene: for everything because the list would be too long to enumerate.

Table of Contents

List of tables	vii
List of Figures	vii
List of abbreviations	viii
Chapter 1: Introduction	1
Myostatin	1
Member of the TGF- β Family	2
Myostatin's role in myogenesis	3
Myostatin and activation of satellite cells	6
Myostatin and growth pathways	7
Myostatin and atrophy pathways	8
Metabolic changes in <i>Mstn</i> ^{-/-} mice	10
Factors affecting muscle growth	10
Factors involved in muscle atrophy	12
Introduction to manuscripts	15
Chapter 2: Myostatin attenuates hyperplasia and is important for muscle remodeling during compensatory growth	16
Abstract	17
Introduction	18
Materials and methods	21

Results	28
Discussion	43
Acknowledgements	51
Chapter 3: Absence of myostatin does not protect skeletal muscles from atrophy induced by denervation	52
Abstract	53
Introduction	54
Materials and methods	56
Results	59
Discussion	64
Acknowledgements	66
Chapter 4: Conclusion	67
References	69
Appendix A: Summary of values used for overload	70
Appendix B: Summary of values used for denervation: Soleus muscle	70
Appendix C: Summary of values used for denervation: Plantaris muscle	70

List of tables

Table 1 Statistical analysis results of morphological changes.....	29
Table 2 Statistical analysis results of MyHC expression.....	32

List of Figures

Figure 1 TGF- β signaling pathway.....	3
Figure 2 Myogenesis and MRFs.....	5
Figure 3 Morphological changes upon overload.....	28
Figure 4 Cross-sectional area of muscle fibers according to major MyHC expression.....	31
Figure 5 Changes in expression of major MyHC isoforms.....	33
Figure 6 Staining for metabolic enzymes SDH and GPDH (Preliminary).....	34
Figure 7 EBD uptake in 3-day overloaded muscles (Preliminary).....	36
Figure 8 Immunofluorescent images of 1-week overloaded muscles (Preliminary).....	37
Figure 9 Embryonic cells after 1 week of overload.....	38
Figure 10 Central nucleation.....	40
Figure 11 Pax7, myoD and myogenin relative protein levels.....	42
Figure 12 Myostatin protein in skeletal muscle, heart and blood serum (Preliminary).....	59
Figure 13 Muscle weights.....	60
Figure 14 CSA of muscle fibers following 2 weeks of denervation.....	62
Figure 15 Expression of major MyHC isoforms after 2 weeks of denervation.....	63

List of abbreviations

Abbreviation	Definition
BrdU	5-bromo-2'-deoxyuridine
BSA	Bovine serum albumin
COX	Cyclo-oxygenase
CSA	Cross-sectional area
DAB	Diaminobenzidine tetrahydrochloride
FoxO	Forkhead box O
GPDH	Glycolytic glycerol-3-phosphate dehydrogenase
IGF-I	Insulin-like growth factor I
MAFbx	Muscle atrophy F-box
MRF	Muscle regulatory factor
MuRF1	Muscle Ring finger 1
MyHC	Myosin heavy chain
OV	Overload
Pax	Paired-box
PBS	Phosphate buffer solution
SDH	Succinate dehydrogenase
TGF- β	Transforming growth factor β

Chapter 1: Introduction

Myostatin

The central dogma as enunciated by Crick tells us that all proteins in living cells come from DNA[1]. The function of proteins ranges from serving as building blocks to regulators and signals of a tight machinery such as myogenesis. Myostatin is such a regulatory protein. It was first discovered during a screen for new members of the Transforming Growth Factor β (TGF- β) superfamily of genes[2]. That same year, it was discovered that a mutation in the myostatin gene was causing a dramatic increase in muscle mass of cattle[2-4]. Natural mutations in the myostatin gene leading to a hypermuscular phenotype have occurred in cattle, sheep and even humans[4-7]. Muscles with the mutation have larger myofibers (hypertrophy) and a greater number of those muscle cells (hyperplasia). Moreover, animals with a non-functioning or absent myostatin gene display a lower fat mass[8, 9]. Gene targeting experiments in mice, where the myostatin gene was removed, have led to a similar phenotype[2]. Due to the therapeutic potentials, extensive research has focused on myostatin's applications[10-14]. Thanks to its effects on skeletal muscle, the removal or inhibition of myostatin is an effective method to treat many pathological states[10, 12, 13]. It has also been shown to be effective in functional improvements in muscular dystrophy[10, 12]. Aged myostatin-null mice display no fiber type changes related to ageing[13]. Additionally, regeneration is accelerated in the myostatin-null mice when compared to the age-matched wildtype mice.

Member of the TGF- β Family

Myostatin is similar in structure and functions the same as the rest of the TGF- β family (Fig. 2). The family is divided into three subfamilies: TGF- β , bone morphogenic protein, and activin[15]. When myostatin is synthesized, it first appears as a precursor protein that contains the active ligand and the propeptide[16]. Once processed, mature myostatin is secreted[2, 16], suggesting a systemic role. The propeptide can bind to the mature myostatin producing an inactive complex that is prevented from binding to response sites[16, 17]. The signaling functions through three main components: the ligand, the receptors, and the intracellular mediators (Smads)[18] (Fig. 1). The signaling begins with the ligand binding to its type II receptor (Fig. 1-1). The type II receptor binds with its corresponding type I receptor (Fig. 1-2&3) and will activate the complex (Fig1-4) and, in turn, activate the Smad protein (Fig. 1-5). The Smad proteins can form a complex with a common Smad termed Smad4 (Fig. 1-6). The Smad complex can enter the nucleus (Fig. 1-7) to regulate transcription in a cell-type-specific manner (Fig. 1-8&9)[19]. Another set of Smads, inhibitor Smads (Smad6 and Smad7) serve to stop TGF- β signaling by an auto-inhibitory loop[11]. In the case of myostatin, the active myostatin ligand binds preferentially to Activin Receptor IIb[20]. It can also bind, with lower affinity, Activin Receptor IIa[20]. The type II receptor will bind to either ALK-5 or ALK-4 receptors[20]. The binding of myostatin to either type II receptors will activate Smad2 and Smad3, then, will form a complex with Smad4. To counteract the myostatin signaling, Smad7 is involved in a negative feedback loop where Smad7 expression is

induced by myostatin and the overexpression of Smad7 leads to inhibition of myostatin[21].

Myostatin's role in myogenesis

Disruption of myostatin signaling induces hyperplasia. The addition of new muscle cells occurs through a process called myogenesis. Myogenesis is involved during development and regeneration following a trauma. It is a process that can be separated into 2 steps: proliferation of cells and differentiation and maturation of proliferated

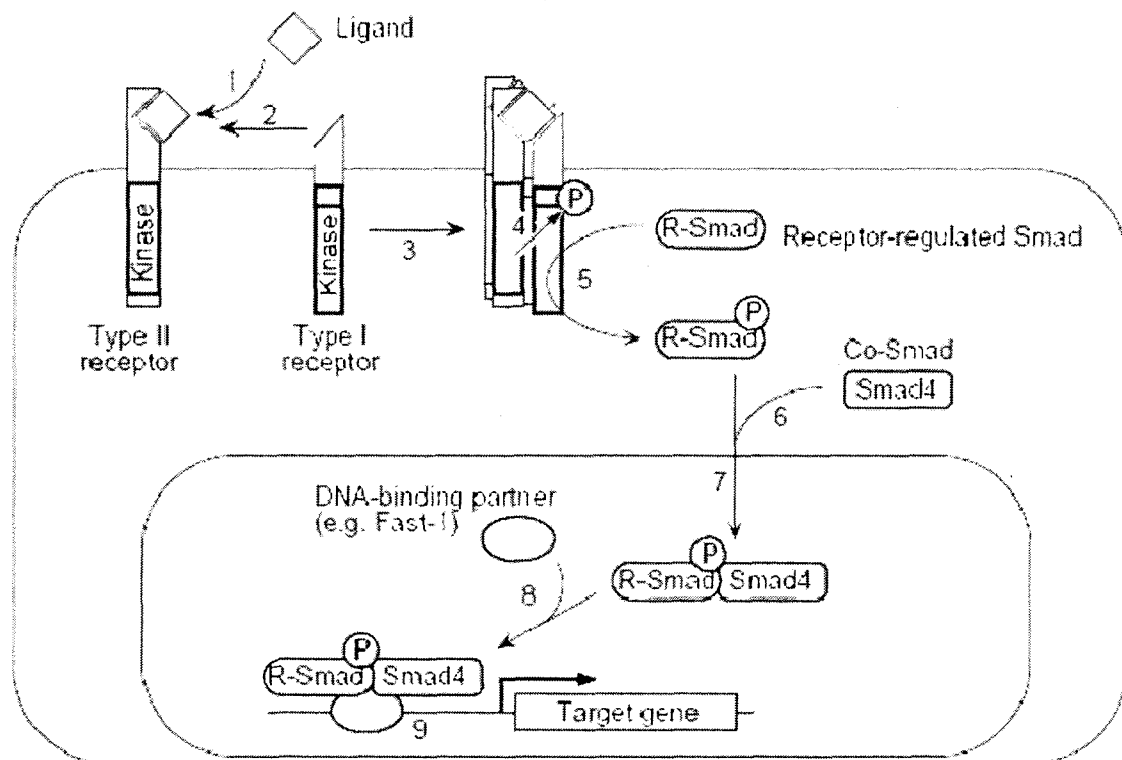


Figure 1 TGF-β signaling pathway

(1) The ligand binds to the type II receptor. (2) The type II receptor associates with the type I receptor. (3) The two receptors form a complex. (4) The complex is activated. (5) The Smad protein is activated. (6) The Smad protein forms a complex with Smad4. (7) The Smad complex enters the nucleus. (8) The Smad complex with a DNA-binding partner binds DNA. (9) The complex initiates the transcription of specific genes. Image taken from [19].

cells. This process is under the regulation of a family of proteins called Muscle Regulatory Factors (MRFs) (Fig. 2)[22-25]. The MRF family includes Myf5, MyoD, myogenin and MRF4[22]. Each of these factors has overlapping but also distinct functions in myogenesis. Indeed, it has been reported that Myf5 enhances myoblast proliferation, whereas MyoD induces differentiation by cell cycle withdrawal[26]. Myogenin is required for the differentiation of myoblasts[27] and MRF4 is thought to be important in the maturation of myotubes[28, 29].

Satellite cells are adult skeletal muscle stem cells that are involved in myogenesis following a trauma[30]. The satellite cells reside beneath the basal lamina juxtaposed to muscle fibers[30]. Under normal conditions, satellite cells remain quiescent but can be activated due to damage caused by mechanical stress[31-34], chemical injection[34] or extreme cold[35]. With a modest stimulus, satellite cells divide, differentiate and can fuse with pre-existing myofibers[30, 34]. In more extreme circumstances, the myoblasts that form after satellite cell division can fuse together and give rise to a new fiber within the basal lamina[32, 33].

The quiescence of the satellite cells is controlled by another regulatory protein called paired-box 7 (pax7)[36, 37]. The Pax genes have important roles in tissue specification and organogenesis such as the central nervous system (Pax2, 3, 5-8), kidneys (Pax2 and 8) and skeleton (Pax1 and 9)[38]. The different functions of the Pax genes include the maintenance of a multipotent state, direction into a differentiation program, cell migration, proliferation, and survival[38]. In skeletal muscles, Pax3 and Pax7 appear to be implicated in these functions in satellite cells. Pax3 is especially

important in the embryo for the migration of muscle progenitors from the somite to more distant sites of myogenesis. Pax3 is also necessary for the activation of Myf5 following this migration to activate the myogenic program[39]. Subsequent myogenesis depends on Pax3 and Pax7. These new cells provide a source of myogenic progenitors for all subsequent muscle growth[38]. During the early postnatal period, approximately 30-35% of nuclei come from satellite cells [40, 41]. Over time, this proportion falls to only 1-4%[42]. Later on, Pax7 is especially important for satellite cell survival and renewal. The removal of Pax7 causes satellite cell death which cannot be substituted by Pax3[37].

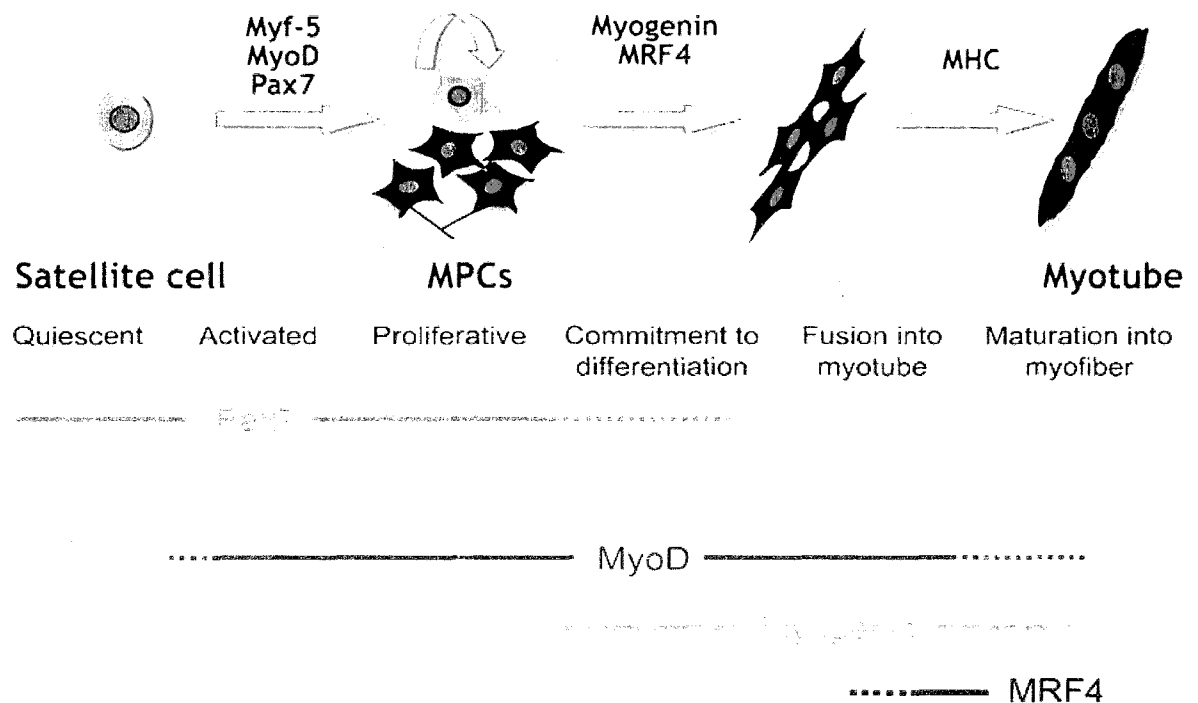


Figure 2 Myogenesis and MRFs

Pax7 maintains satellite cell quiescence, but upon activation, the primary MRFs, Myf5 and MyoD, are required for myogenic determination, whereas, the secondary MRFs, myogenin and MRF4, are required for differentiation. Image adapted from [43, 44].

To understand the mechanism by which myostatin regulates muscle mass, gain and loss of function analysis was done in cell culture. Myostatin addition to the cell culture inhibits myoblast proliferation and differentiation[45-47]. This inhibition is also dose-dependent[45]. Myostatin prevents the progression of myoblasts through the cell cycle[45]. Smad3 is known to interfere with MyoD[48], and therefore, the reduction in activity of MyoD could interrupt the cycle[47].

Myostatin and activation of satellite cells

Myostatin is present in satellite cells and myoblasts[49]. Not surprisingly, increased activation of satellite cells occurs in the absence of myostatin[49]. It is also important to note that, *in vitro*, myoblasts from *Mstn*^{-/-} mice stopped proliferating and differentiated into myoblasts much later than myoblasts taken from wildtype (*Mstn*^{+/+}) mice. In the *Mstn*^{-/-} myoblasts, myoD is expressed for a longer period of time and the induction of myogenin is delayed when compared to the wildtype (*Mstn*^{+/+}) counterpart[49]. Additionally, myostatin signals through Pax7 to regulate satellite cell renewal[50]. Myostatin addition severely downregulates Pax7 expression and absence of myostatin causes an upregulation in Pax7[50]. *In vitro*, cells from myostatin-null mice display higher levels of Pax7[50]. During differentiation, lack of myostatin results in an increased pax7 expression and those elevated levels are maintained considerably longer[50]. More recently, a controversial study found that the loss of myostatin does not lead to increased satellite cell activation and the increased muscle mass is mostly a result of hypertrophy[51]. As mentioned previously, myostatin's inhibitory action on

satellite cells is dose-dependent; however, the concentration used in the latest study was below a concentration where no effect was previously observed[45, 47].

Myostatin and growth pathways

One of the best known growth-promoting factor is the insulin-like growth factor, IGF-I. IGF-I is synthesized in the liver under growth hormone (GH) control[52]. The induction of hypertrophy by IGF-1 is dependent on a pathway initiated by phosphatidylinositol-3-kinase (PI3K) which regulates Akt. Targeted activation of Akt also leads to muscle growth[53, 54]. Surprisingly, Akt activation does necessarily occur through the IGF receptor following increased mechanical loading on skeletal muscle[55].

Moreover, IGF-I is thought to induce the activation of satellite cells[56]. Most of the data is restricted to cell culture, however, muscle hypertrophy by delivery of IGF-I is blocked by irradiating the muscle[57]. Irradiation is thought to prevent satellite cell activation, however, little is known about the non-specific effects on other cell types[58, 59]. A recent study has shown that Akt activation does not lead to satellite cell activation[60]. The authors did not, however, label satellite cells to determine the amount of growth attributable to satellite cell activation. Myostatin has also been found to interact with the IGF pathway (Fig. 3). *In vitro*, overexpression of myostatin attenuates myotube growth and reduced Akt phosphorylation[61, 62], whereas the absence of myostatin is sufficient to induce growth[61]. Inhibition of Akt phosphorylation also blocks myotube hypertrophy even in the absence of myostatin[61].

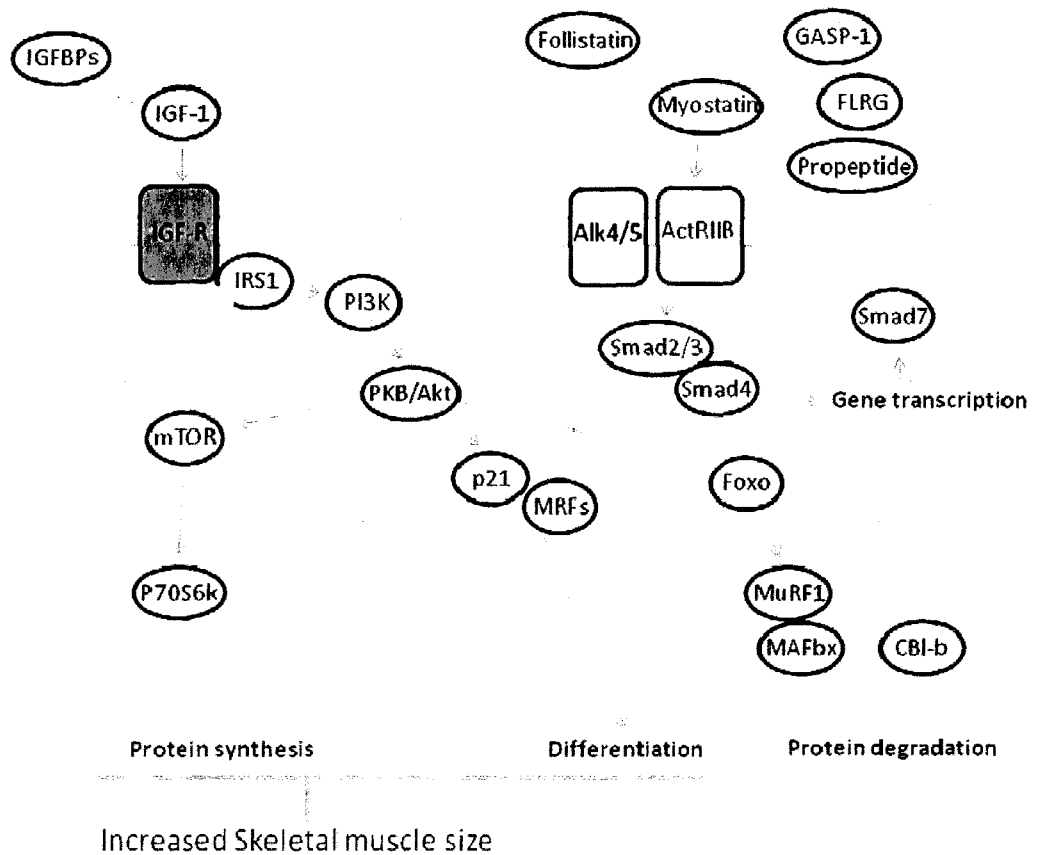


Figure 3 Myostatin and IGF signaling interactions

Many interactions are known to exist between the myostatin and IGF pathways. Redundancies are found at different levels and act the pathways in concert to balance the size of skeletal muscle. Image modified from [63].

Myostatin and atrophy pathways

Atrophy is defined as a decrease in cell size mainly caused by a loss of organelles, cytoplasm and proteins[64]. In the case of skeletal muscle, atrophy occurs when the rate of protein degradation exceeds the rate of protein synthesis[65]. Gene expression comparison in different models of atrophy shows a subset of genes commonly up- and downregulated in muscle. These genes that are common to all atrophy models are called atrophy-related genes or atrogenes[66], suggesting a process controlled by

specific signaling pathways. The two most induced genes in skeletal muscle specifically are responsible for protein degradation: atrogin-1 and MuRF1[67, 68].

Atrogin-1 and MuRF1 are known to induce protein degradation by using the ubiquitin-proteasome system[67]. In this system, proteins are tagged and degraded by a proteasome[69, 70]. The specificity of the tagging is due to the ubiquitin ligases which

contain a specific target-recognition subunit[69]. Atrogin-1 and MuRF1 are ubiquitin ligases. Some of the identified targets of atrogin-1 are MyoD and myogenin[71, 72].

Importantly, recent findings suggest MuRF1 is involved in the degradation of MyHCs[73]. The knockout of either MuRF1 or atrogin-1 makes mice partially resistant to atrophy.

Under atrophic conditions, treatment with IGF-I results in reduced activation of MuRF1 and atrogin-1[74, 75]. Akt can stimulate skeletal muscle hypertrophy but also inhibits atrophy. The mechanism by which Akt regulates atrogin-1 and MuRF-1 involves the FoxO family of transcription factors [74, 75]. Phosphorylation of FoxO proteins promotes the export of FoxOs from the nucleus to the cytoplasm. Upon dephosphorylation, FoxO proteins translocate to the nucleus[76]. Accordingly, mice overexpressing FoxO1 show a markedly reduced muscle mass, further supporting the role of FoxO in atrophy[77].

In many different models of atrophy such as disuse, denervation, disease and sarcopenia, myostatin is increased[78-81]. A link between myostatin's function and atrophy was found through FoxO1. FoxO1 can bind to myostatin's promoter region and increase the expression of myostatin[82]. This effect can be potentiated in the presence

of Smad proteins[82]. Furthermore, myostatin treatment induces cachexia by inhibiting Akt phosphorylation and thereby increasing levels of active FoxO1[83]. This suggests that myostatin is involved a feed forward mechanism where myostatin increases FoxO's activation, which in turn, increases myostatin's expression.

Metabolic changes in *Mstn*^{-/-} mice

Changes in the expression of different isoforms of the major contractile protein of skeletal muscles, myosin, have also been observed. Myostatin-null mice have a greater proportion of fast glycolytic fibers in all skeletal muscles studied[84-86]. Interestingly, in animals expressing normal levels of functioning myostatin, fast muscles express more myostatin and this expression is highly correlated with the proportion of fibers displaying MyHC IIb[81]. MyoD, a muscle regulatory factor, preferentially expresses MyHC IIb. In turn, myostatin-null mice express higher levels of MyoD[86]. It has been indeed shown that MyoD is one of myostatin's targets[47, 86]. To further support myostatin's role in the switch towards a faster glycolytic phenotype, functional assessment of ATPase and succinate dehydrogenase (SDH) activity confirms a shift towards a faster and more glycolytic phenotype in myostatin-null mice[85]. Furthermore, the number of mitochondria is reduced[85].

Factors affecting muscle growth

Functional overload involves surgical removal of synergistic muscles causing a rapid growth response that leads to increased muscle mass, greater muscle midbelly and fiber cross-sectional area and protein synthesis[87-91]. In two to four weeks of

overload, the plantaris mass almost doubles[91]. These changes are also marked by a change in myosin heavy chain expression that follows a fast-to-slow transition[89, 90].

The time-course of changes following the compensatory response to removal of synergistic muscles occurs in two distinct phases: an immediate short-term inflammatory reaction and a slower long term adaptation to the elevated demands on the muscle[92].

The initial phase involves increased water content and invasion of the muscle by inflammatory cells[92]. The invasion is very rapid since two hours is sufficient to detect significant changes in the population of neutrophils[93]. The peak response occurs within the first 24 hours and is maintained up to five days post-surgery, after which the response declines[92]. By two weeks after the surgery, the levels of inflammation are back to normal. At the same time, markers of myogenesis become significantly higher after just 12 hours of overload[94].

Further on, the anabolic effects of IGF-I are well known. IGF-I can induce hypertrophy both *in vitro* and *in vivo*[95, 96]. Insulin-like growth factor I (IGF-I) is also upregulated 3 days following overload[97, 98] and its downstream target Akt becomes phosphorylated[54]. This increase in the growth factors is growth-hormone independent[98]. However, IGF-I has also been found to be dispensable to induce hypertrophy following functional overload[55]. The rapid initial growth has also been attributed in part to the proliferation of satellite cells[59]. Following, hypertrophy, the ratio of nuclei to cytoplasmic volume is maintained and it would therefore require new cells to donate their nuclei[57, 99]. Since muscle is formed of post-mitotic cells,

hypertrophy is dependent on activation of satellite cells and their fusion into existing myofibers[100].

Following the acute response to overload, slower adaptations in the morphological and biochemical structure will occur. The changes in MyHC expression are extensively described with significant differences after only two weeks[89, 91, 101]. During that time frame, the expression of MyHC IIa is already increased and remains high. After four weeks, the proportion of fibers expressing MyHC I increases as well. The reduction in MyHC IIb is apparent after six weeks of overload. Changes in activity of different enzymes are coordinated with the expression of distinct MyHC isoforms following functional overload. The oxidative enzyme SDH activity increases, whereas the glycolytic glycerol-3-phosphate dehydrogenase (GPDH) activity declines[89]. Recently, a few studies have tried to determine the capacity of the genetically altered mice to perform exercise and to adapt to the functional demands[102-104]. *Mstn*^{-/-} mice have a reduced exercise capacity; however, the amount of daily exercise performed varies among the studies[103, 104]. More importantly, the muscles of *Mstn*^{-/-} mice maintain their plasticity to meet the functional demands[102, 103].

Factors involved in muscle atrophy

Denervation through sciatic nerve section is an effective method to induce atrophy. Similar to all disuse models, 2 weeks of denervation in rodents causes a reduction in muscle mass between 30-50% with a concordant change in individual fiber size[66, 79,

105]. Just as in overload, changes in MyHC expression also occur; however, discrepancies exist among the studies as to the direction of the switch[105-108]. Denervation atrophy has an initial rapid, then slow phase[66, 79]. During the first two weeks, up to 50% of the muscle mass is lost. Longer studies up to eight weeks show no additional loss[66, 79].

Many genes are differentially expressed during the initial phase. MuRF1 and MAFbx are among the mRNA most drastically induced by denervation[66, 109, 110]. These atrogenes start rising after one day of denervation, reaching their peak at three days[66]. The expression of those genes is dependent on the FoxO family of transcription factors, FoxO1 and FoxO3a[74, 109, 111]. FoxO3a directly binds to the MAFbx promoter region and induces its transcription; whereas FoxO1, synergistically with the glucocorticoid receptor, induces the expression of MuRF1. Although, the levels of MuRF1 and MAFbx return to basal levels after 14 days, FoxO1 can remain elevated up to 28 days following surgery[66]. Besides protein degradation, apoptosis also contributes to muscle mass loss[112]; however, the earliest time point where apoptosis can be detected is two months[113].

Changes in the expression of the different isoforms of MyHCs are well described in rats[106, 114]. The direction of the change depends on the predominant fiber type of the muscle prior to denervation[106, 115]. Fast muscles develop a tendency towards a slower phenotype and slow muscle show a shift towards a fast phenotype. The effect of denervation on mice appears to differ from rats since mice do not lose MyHC I[105].

However, mice still show a reduced oxidative capacity, typical of denervation-induced atrophy.

In wildtype animals, myostatin expression levels rise very rapidly and peak after three days of denervation[79]. The protein levels peak at seven days and remain elevated up to 28 days[79]. A similar trend can be seen in myostatin's downstream target, the phosphorylated Smad2[79]. As mentioned previously, myostatin's expression is muscle specific and its expression correlates with the percentage of MyHC IIb isoforms expression[81]. In fact, no myostatin is found in the soleus muscle[81]. It is not upregulated in soleus either when atrophy is induced by hindlimb unloading[81] suggesting an alternative pathway. Different models of atrophy consistently lead to an upregulation of myostatin[78, 81, 116-120].

Introduction to manuscripts

The following chapters are manuscript to elucidate myostatin's role in regulating muscle fiber size. We used the myostatin knockout model to assess whether absence of myostatin 1) enhances muscle growth when forced to hypertrophy and 2) protects skeletal muscles from atrophy.

Myostatin is involved in satellite cell activation and in growth pathways. No study up to date has focused on the capacity of myostatin-null mice to activate satellite cells following synergist ablation. Myostatin is downregulated following functional overload[98]; however, the capacity of these muscles to undergo the changes that occur in the absence of myostatin has not been determined. I hypothesize that functional overload will induce a potentiated growth in myostatin null mice. This growth would be a result mostly due to greater hyperplasia.

As mentioned previously, myostatin is upregulated in different models of skeletal muscle atrophy. Treatments targeting the myostatin pathway can also partially prevent atrophy. However, the effects of constituent knockout of myostatin on denervation have not been studied so far. I hypothesize that muscles from *Mstn*^{-/-} mice will be spared from atrophy normally observed following denervation.

Chapter 2: Myostatin attenuates hyperplasia and is important for muscle remodeling during compensatory growth

Manuscript in preliminary phase of preparation

Abstract

Myostatin is a negative muscle mass regulator part of the TGF- β family of growth factors. The increase in muscle mass is a result of hypertrophy and hyperplasia. To investigate the role for myostatin (Mstn) in muscle fiber remodeling, we compared the effects of functional muscle overload of the plantaris in Mstn Knockout (Mstn $-/-$) and wildtype (Mstn $+/+$) mice. The muscle midbelly area of non-overloaded (OV) Mstn $-/-$ mice was double that of Mstn $+/+$ counterparts due to a higher number of muscle fibers and fibers displaying greater cross sectional size. Six weeks of functional overload led to a blunted growth marked by significant differences in the increase in mean midbelly area (Mstn $+/+$: 90%; Mstn $-/-$: 23%; $p < 0.05$). The blunted growth was concomitant with increases in individual fiber sizes (Mstn $+/+$: 35%; Mstn $-/-$: 8%; $p < 0.05$). Additionally, muscles from Mstn $-/-$ mice maintain the plasticity to adapt to functional demands as marked by changes in the expression of the different isoforms of MyHC, however, that response was also blunted. Following the surgery, the distal portion of the plantaris muscle was a region of major remodeling in both groups. Compared to their wildtype (Mstn $+/+$) counterparts, Mstn $-/-$ mice displayed more damage marked by EBD and more regeneration marked by 5-bromo-2'-deoxyuridine (BrdU) and myogenin. This differential growth pattern may be of importance when considering Myostatin-related therapies in aging and diseases such as muscular dystrophy. Funded by CIHR, NSERC and CRC.

Introduction

Myostatin is a negative muscle mass regulator part of the TGF- β family of growth factors[121, 122]. Natural mutations in the myostatin gene leading to a hypermuscular phenotype have occurred in cattle, sheep and even humans[4-7]. Mice lacking myostatin display a doubling in muscle mass as a result of hyperplasia and hypertrophy[122]. By binding to its receptor, activin IIb receptor[123], myostatin inhibits the proliferation and differentiation of muscle fibers. This effect was also observed *in vitro* using c2c12 cells[124, 125]. Following the binding of myostatin to its receptor, a signaling cascade involving Smad proteins[126, 127] begins and results in the inhibition of the growth PKB/AKT pathway and activation of the atrophy pathway through the forkhead box O (FOXO) transcription factor and Muscle Ring Finger 1 (MuRF1) / Muscle Atrophy F-box (MAFbx) (also known as atrogin-1)[128-131].

Plantaris muscle functional overload is a well established model to study muscle growth in rodents[88, 132]. It is achieved by removing synergist soleus and gastrocnemius muscles. The changes following the surgery occur in two distinct phases. The long term changes are well documented and are characterized by increased muscle mass, greater midbelly area, an increase in midbelly fiber size as well as protein synthesis[133, 134]. The muscle fibers also undergo a transition from fast, glycolytic, to slower, more oxidative energy efficient phenotypes. In rodent fast muscle, the myosin heavy chain enzyme component of myosin follows a conversion pattern in response to overload from the fastest to the slowest isoform in the order: MyHC IIb \rightarrow IIx \rightarrow IIa \rightarrow I/slow[135-137]. In control plantaris muscles, cells expressing the various MyHCs display

distinct metabolic profiles[89]. Muscle fibers expressing MyHC IIa have a greater mean SDH activity than all other isoforms in the order: IIa → I → IIx → IIb. As for GPDH activity, fibers expressing MyHC IIb and IIx have the greatest mean activity followed by fibers expressing MyHC IIa and I. Changes in activity of metabolic enzymes are also coordinated with the expression of distinct MyHC isoforms following functional overload. The oxidative enzyme SDH activity increases, whereas the GPDH activity declines[89]. Most recently, studies have demonstrated that *Mstn*^{-/-} muscles maintained the plasticity to increase their oxidative capacity following exercise[102, 103].

The initial phase following the surgical ablation involves increased water content and invasion of the muscle by inflammatory cells[92]. The peak response occurs with 24hrs and is maintained up to five days post surgery. By two weeks, the levels of inflammation are back to normal[92].

The literature on muscle damage following functional overload is limited due to the confounding inflammation, however, unloading/reloading, stretch and eccentric contractions are known to cause muscle damage[31, 138, 139]. Most importantly, the location of the injury and regeneration remains consistently in the distal portion of the plantaris muscle[138]. Interestingly, proliferating cells were found mostly in the distal regions of plantaris muscle in overload rats[140]. Muscle regeneration after injury has similarities to muscle development during embryogenesis and seems to follow the same procedure[141]. Muscle satellite cells, normally located within the basal lamina of the muscle, become activated, proliferate and differentiate to become mature muscle

fibers. Following differentiation, satellite cells can incorporate their nuclei into pre-existing fibers to repair damaged fibers[142, 143]. Interestingly, satellite cells were found to be more concentrated at the ends of growing muscle fibers[144]. In their quiescent state, satellite cells are found to express Pax7 and/or Myf5[145-148]. The population of satellite cells in muscles remains fairly constant throughout adult life which requires the satellite cells to possess a self-renewal capacity, a phenomenon still poorly understood[149, 150]. One of the stimuli known to activate satellite cells is functional overload[151].

To better understand Myostatin role in growth, we subjected wildtype (*Mstn*^{+/+}) and *Mstn* Knock-out mice (*Mstn*^{-/-}) to functional overload for different periods of time. We hypothesized the plantaris of OV *Mstn*^{-/-} mice would have a potentiated growth response implicating muscle satellite cells compared to *Mstn*^{+/+} OV counterparts.

Materials and methods

Animal care and protocols

All animal care and experimental procedures were performed in accordance with the guidelines established by the Canadian Council of Animal Care. These procedures were approved by the University Animal Research Ethics Committee (UAREC) of Concordia University. *Mstn*^{-/-} mice were kindly donated by Dr. S.-J. Lee. (Johns Hopkins University School of Medicine, Baltimore, MD)

Animal surgeries

All surgical procedures were performed under aseptic conditions on animals anesthetized by intramuscular injection (1.2 µl/g) of 100 mg/ml ketamine hydrochloride and 10 mg/ml xylazine in a volume ratio of 1.6:1. For OV experiments, compensatory hypertrophy of the plantaris was induced in each limb in *Mstn*^{+/+} and *Mstn*^{-/-} mice by surgically ablating the soleus and a major portion of the gastrocnemius muscle. The mice were overloaded for periods of 24 hours, 3 days, 7 days, 14 days or 42 days. Following the surgeries, the mice were given children's ibuprofen diluted in water for the first 3 days. No ibuprofen was added for the rest of the duration of the functional overload period. After a period of convalescence (3-7 days), the OV mice were exercised daily for 60 minutes by placing them in an exercise ball (12 cm diameter). Plantaris, Tibialis anterior, Extensor digitorum longus muscles from control or overloaded mice were excised and either frozen directly in liquid nitrogen or embedded in OCT (Tissue-Tek, Torrance, CA) and frozen in melting isopentane before being put in liquid nitrogen. Tissues were stored at -86°C until processed.

Cell nuclei labeling

During cell division, DNA is replicated to generate 2 identical cells. 5-bromo-2'-deoxyuridine (BrdU), a synthetic nucleoside, can substitute for thymidine during DNA replication [152]. The inserted BrdU can then be labeled with a specific antibody, thus indicating the nuclei that have undergone DNA replication. The proliferation in the 3-day overloaded plantaris muscle was assessed by the uptake of BrdU [91]. Briefly, 50mg/kg of body weight was injected daily intraperitoneally. The first injection was administered following the overload surgery; the others were done at 24 hour intervals and the last, 2 hours prior to extraction.

Immunohistochemistry

Antibodies used were: MyHC I: A4.840, (1:25, Developmental study hybridoma bank (DSHB), University of Iowa, Iowa city, IA); MyHC IIa: SC71 (1:12.5; DSHB); MyHC IIx: 6H1 (undiluted; DSHB); MyHC IIb: BF-F3 (1:25; DSHB); MyHC emb I: F1.652 (1:10; DSHB); MyHC emb II: 47A (1:10; DSHB); anti-mouse HRP : IgG A8924 (Sigma-Aldrich) or IgM A8786 (Sigma-Aldrich). To determine the MyHC isoform expressed by each fiber, cryosections (10 μm) were cut from the same anatomical location in each muscle midbelly and recovered onto Superfrost[®] Plus microscope slides (Fisher Scientific). First, the sections were blocked in 5% goat serum in a carrier solution consisting of 0.5% bovine serum albumin (BSA) in 25 mM phosphate buffer solution (PBS) (pH = 7.4) for 30 minutes. The sections were then probed overnight at 4°C in carrier solution with one of the following primary antibodies raised against the different MyHC types (I, IIa, IIx, IIb, Embryonic). After three 10-min PBS rinses, sections were then probed at room temperature with either horseradish

peroxidase-conjugated anti-mouse IgG (MyHC type IIa, 1:25; Embryonic, 1:50) or IgM (MyHC type I, IIx, IIb; 1:25) (Sigma-Aldrich). The sections were rinsed three times with PBS for 10 minutes. The bound antibody complexes were then visualized using diaminobenzidine tetrahydrochloride (DAB) as per the manufacturer's instructions (Thermo Fisher Scientific, Rockford, IL). DAB makes the bound peroxidase-conjugated antibodies turn brown and can be visualized with a light microscope.

Three to five distinct regions were selected randomly from the midbelly of each plantaris muscle. All fibers in those regions were identified across each serial tissue section with the aid of a Retiga SRV camera (QImaging, Surrey, BC, Canada) mounted on an Olympus BX-60 (Olympus, Center Valley, PA) microscope. Each area of interest comprised approximately 75 fibers. The images were analyzed using ImagePro Plus version 6.2 software (Media Cybernetics, Bethesda, MD). Fibers were classified according to their staining profile with the distinct antibodies. For consistency, cell size was measured on a single non-stained muscle section fixed with 1% paraformaldehyde for 20 minutes in PBS followed by 3 washes in PBS for 5 minutes each.

For central nucleation, muscles cryosections (10 μm) were obtained and recovered on Superfrost® Plus Slides. The slides were processed for hematoxylin and eosin staining, dehydrated and mounted. Images were captured covering the whole belly and all muscle fibers were classified according to the number of centrally located nuclei. Results were normalized to the belly area.

SDH and GPDH activity

SDH and GPDH activity was measured as described previously[136]. All images were captured with the aid of a Retiga SRV camera mounted on an Olympus BX-60 microscope. OD analysis was completed using ImagePro Plus version 6.2. For SDH, serial sections (14 μ m) of muscle were cut from the plantaris muscle midbelly and were adhered to slides. The slides were placed under a microscope. The tissue was first incubated in the dark at 23°C in a substrate-free blank solution consisting of 1 mM sodium azide, 1 mM l-methoxyphenazine methosulfate (MPMS), 1.5 mM NBT, and 5 mM EDTA in 100 mM sodium phosphate buffer (pH 7.6). The reaction was allowed to proceed for 10 min to allow for endogenous staining to plateau. The blank was then replaced with a substrate solution consisting of the above reagents plus 48 mM succinic acid. Images were captured every 2 min for 10 min. During this time, increases in optical density (OD) are linear (data not shown).

For measurement of single fiber GPDH activity, serial sections (14 μ m) were cut, adhered to slides, and distributed between two coplin jars kept at -20°C. A blank solution consisting of 1 mM sodium azide, 1 mM MPMS, 1.2 mM NBT in 100 mM sodium phosphate buffer (pH 7.4, 37°C) was added to one jar while a solution of the above reagents plus 9.3 mM α -glycerophosphate was introduced into the other for the substrate reaction. Tissue sections were incubated in the dark for 24 min at 37°C. The reactions were then stopped by extensive rinsing with distilled water (5 times plus 3 x 1 min). Sections were air-dried and mounted with glycerine (Sigma). Images of the blank and end-point substrate reactions were captured and processed for OD analysis.

The average grayness for all pixels within this traced area was determined across all saved sequential images and converted to an OD value. The enzyme specific activities were expressed as the change of OD over time (OD/min; average $r^2 \geq 0.99$). The cross-sectional area of each traced cell was also determined from these images. The total enzyme activity within each cellular tissue section was calculated by multiplying the CSA of each fiber by its specific enzyme activity. The CSA of each whole midbelly section was also determined using this same system for comparison among groups.

Evans Blue Dye staining

To visualize muscle fibers that sustained injury following overload, Evans blue dye was injected as described previously[93]. Briefly, 24 hours prior to muscle extraction, animals were injected intraperitoneally with 100 mg/kg body weight of Evans Blue Dye (5% w/v of Evans Blue in PBS, pH = 7.4). Evans blue binds to albumin and other serum proteins which normally are impermeable to cell membranes. Muscle fibers that sustained damage to their membrane will absorb the albumin bound to the dye[153], where it can be visualized by fluorescence microscopy at an emission of 515 nm. To determine the location of the damage, thick sections (20 μm) were obtained at the midbelly and 2 mm distal from the midbelly close to the Achilles tendon. For longitudinal sections, the plantaris muscle was oriented to obtain sagittal sections. Once recovered on a slide, each muscle section was quickly covered with cold EDTA (4°C, 0.5M, pH 8.0) for 30 seconds. Following abundant washes (10x30seconds), the slides were dried and covered with glycerine. As control for EBD staining, we injected mdx mice displaying a similar but less severe phenotype of Duchenne muscular dystrophy.

Protein extraction and immunoblotting

Antibodies used were: Pax7, 1:10: PAX7 (DSHB); Myogenin, 1:10: F5D (DSHB); MyoD, 1:1000: C-20 (Santa Cruz Biotechnology); alpha tubulin, 1:2000: 2125 (Cell Signaling Technology); anti-mouse HRP, 1:1000: A8924 (Sigma-Aldrich); anti-rabbit HRP, 1:1000: 7074 (Cell Signaling Technology). Muscles were homogenized in RIPA buffer [PBS (pH 7.4), 1% Igepal, 0,5% Sodium deoxycholate, 0,1% SDS, 10 µg/ml leupeptin, 10 µg/ml aprotinin, 1 mM 4-(2-aminoethyl)benzene sulfonyl fluoride, 10 mM NaF, and 1 mM sodium ortho vanadate] using a TissueTearor homogenizer (ColeParmer, Montreal, QC) at low speed for 45 seconds. Homogenates were centrifuged at 13 000 x *g* for 30 min at 4°C to pellet cell debris. The supernatant was quantified using the QuickStart Bradford dye reagent (Bio-Rad, Mississauga, Ontario, Canada). For protein analysis, 150 µg protein were resolved by SDS-PAG, transferred to a PVDF membrane (Millipore). The protein/antibody complex was revealed by chemiluminescence using the Immobilon Western kit (Millipore).

Immunofluorescence

Antibodies used were: Myogenin, 1:50: G20 (Santa Cruz Biotechnology Inc, santa Cruz, CA); BrdU, 1:50, 250563 (Abbiotec, San Diego, CA); anti-goat Alexa488, 1:100, A11055 (Invitrogen, Burlington, ON); anti-rabbit Alexa546, 1:100, A11010 (Invitrogen). 10 µm sections of plantaris muscles were recovered onto Superfrost[®] Plus microscope slides (Fisher Scientific). The tissue sections were then fixed with 2% paraformaldehyde for 20 minutes (Sigma-Aldrich) and washed 3 times (5 minutes each) with PBS. Sections were blocked and

permeabilized with 2% normal goat serum (Sigma-Aldrich) and 0.2% Triton X-100 (Sigma-Aldrich) for 1 hour. Sections were then incubated overnight at 4°C with the antibodies listed previously in PBS containing 1% normal goat serum and 0.05% Triton X-100. Slides were then washed 3 times with PBS and secondary antibodies as listed previously were applied for 1 hour at room temperature in PBS containing 1% normal goat serum and 0.05% Triton X-100. Slides were washed 5 minutes 3 times and air-dried. Sections were mounted in Vectashield containing 1.43nM DAPI (Vector Laboratories, Burlington, ON). Control experiments omitting primary antibodies revealed absent or very low-level background staining. Images were acquired on an Olympus BX-60 fluorescent microscope (Olympus) using Image-pro 6.2 software (Olympus).

Statistical analysis

The data was tested for homogeneity of variance, and in the case where homogeneity was found, a two-way ANOVA was used. LSD was used as a *post hoc* test when appropriate. When the variance between the groups was not homogenous, the Kruskal-Wallis test was performed. The statistics were done with computer assistance using SPSS Statistics GradPack version 17.0.

Results

Comparison of control phenotypes

The muscle midbelly area and muscle weight of the control *Mstn*^{-/-} plantaris muscle was significantly greater when compared to the *Mstn*^{+/+} mice (Fig. 4A & C) (midbelly area: 67% and muscle weight: 76%; $p < 0.05$). Even when controlled for the greater body weight, the relative muscle weight of the *Mstn*^{-/-} was still significantly higher (Fig. 4C) (55%; $p < 0.05$). This was due to a greater number of muscle fibers (30%) and also larger individual cross-sectional areas (29%) (Fig. 4D). Additionally, the proportion of muscle

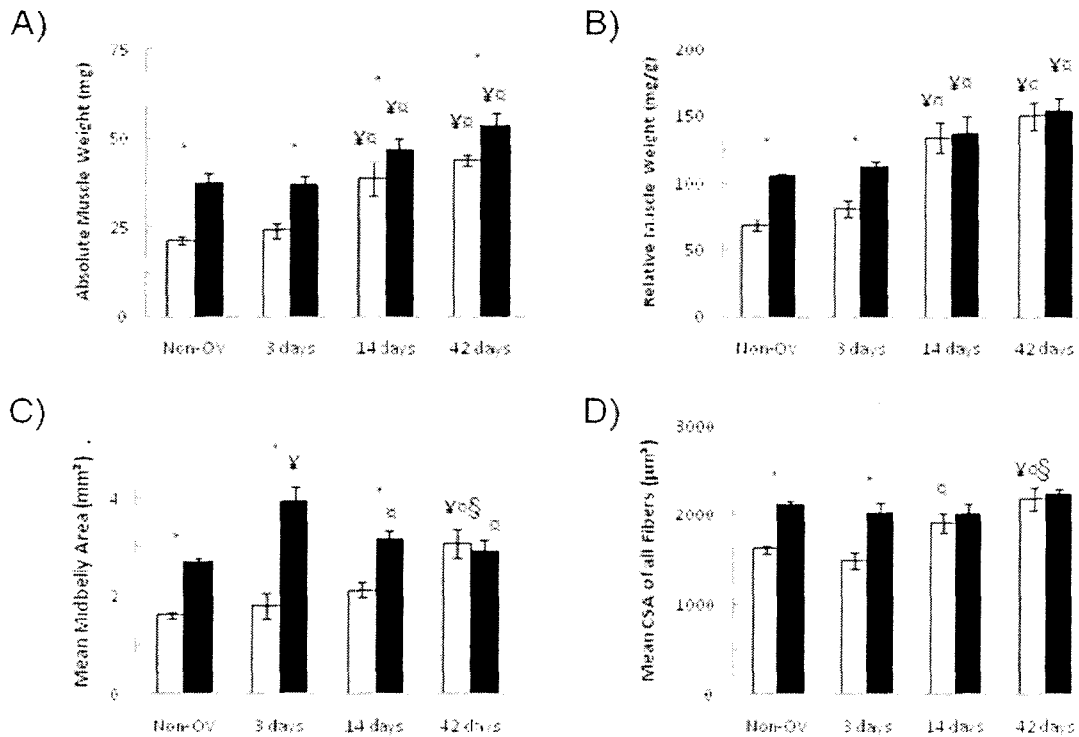


Figure 4 Morphological changes upon overload

A) Absolute muscle weight over the time-course in *MSTN*^{+/+} (open bars) and *Mstn*^{-/-} (closed bars) mice. B) Plantaris absolute muscle weight relative to body weight. C) Mean midbelly area. D) Mean cross-sectional size of individual fibers irrespective of the MyHC expressed. Values for all graphs are means \pm S.E. $n=4-7$ per treatment group. * different ($p < 0.05$) from wildtype (*Mstn*^{+/+}) counterpart, † different ($p < 0.05$) from non-overloaded control, ‡ different from 3-day overloaded muscles, § different ($p < 0.05$) from 2-week overloaded groups.

fibers expressing MyHC IIa (42%; $p < 0.05$) compared to wildtype (*Mstn*^{+/+} mice (Fig. 5). fibers expressing MyHC IIb was greater in *Mstn*^{-/-} (42%; $p < 0.05$) and less of the smaller *Mstn*^{-/-} plantaris muscles did not show any fibers expressing MyHC type I.

Muscle morphological changes

The results of the statistical analysis related to the changes observed can be found in table 2. As expected, 2 and 6 weeks of functional overload resulted in significant increases in absolute plantaris muscle mass (Fig. 4A) for both groups with no significant differences between the groups (*Mstn*^{+/+}: 82-105%; *Mstn*^{-/-}: 25-42%; $p < 0.05$). After controlling for the body weights, a tendency for *Mstn*^{-/-} to grow less in relative muscle mass was observed (Fig. 4B). The changes in relative muscle weight corresponded to increases in the mean cross-sectional size of all plantaris MyHC-typed fibers (Fig. 4D).

Table 1 Statistical analysis results of morphological changes

p-values for the main effects and interactions of each variable. Asterisks denote significance ($p < 0.05$)

Variable	KO effect	OV effect	Interaction
Muscle mass:			
Absolute	<0.001*	<0.001*	0.529
Relative	0.004*	<0.001*	0.084
CSA of fibers expressing:			
All fibers combined	<0.001*	0.001*	0.044*
MyHC I	0.306	0.011*	0.604
MyHC IIa	0.196	<0.001*	0.018*
MyHC IIx	0.371	<0.001*	0.026*
MyHC IIb	0.497	0.005*	0.130
Midbelly Area	<0.001*	0.004*	0.001*
Cell Count	<0.001*	0.008*	0.003*

Significant interactions were found in the growth response where the mean CSA of fibers in *Mstn*^{-/-} mice did not increase as much as the wildtype (*Mstn*^{+/+}) counterparts. Further on, differences in the individual fiber type classifications varied depending on the major MyHC expressed (Fig. 5). Significant increases in CSA were found in all fiber types; however, only fibers expressing MyHC IIa and IIx displayed a blunted growth response in the *Mstn*^{-/-} group. Differences in size of fibers expressing MyHC IIb were more modest and therefore no significant interaction was found. The comparison of the CSA of fibers expressing MyHC I could not be completed between the *Mstn*^{-/-} and *Mstn*^{+/+} mice since no fibers were present in the *Mstn*^{-/-} mice at 0 and 3 days. Two weeks after the surgery, only one mouse was found to have fibers expressing MyHC I. For the mean midbelly area (Fig. 4C), significant interactions were found ($p < 0.05$). Mean midbelly area grew by 112% ($p < 0.05$) in the wildtype (*Mstn*^{+/+}), whereas the *Mstn*^{-/-} only grew by 23%. A drastic increase in midbelly area (46%; $p < 0.05$) was observed in *Mstn*^{-/-} mice 3 days following surgery most likely due to some inflammatory response in this group. To evaluate hyperplasia, the estimated cell count was obtained by dividing the mean midbelly area by its corresponding mean cross-sectional size of the individual fibers. The number of fibers increased significantly only after 6 weeks of overload in the wildtype (*Mstn*^{+/+}) mice. In *Mstn*^{-/-}, a smaller non-significant increase was found. The large increase at 3 days in the *Mstn*^{-/-} group most likely reflects the inflammation due to the surgery.

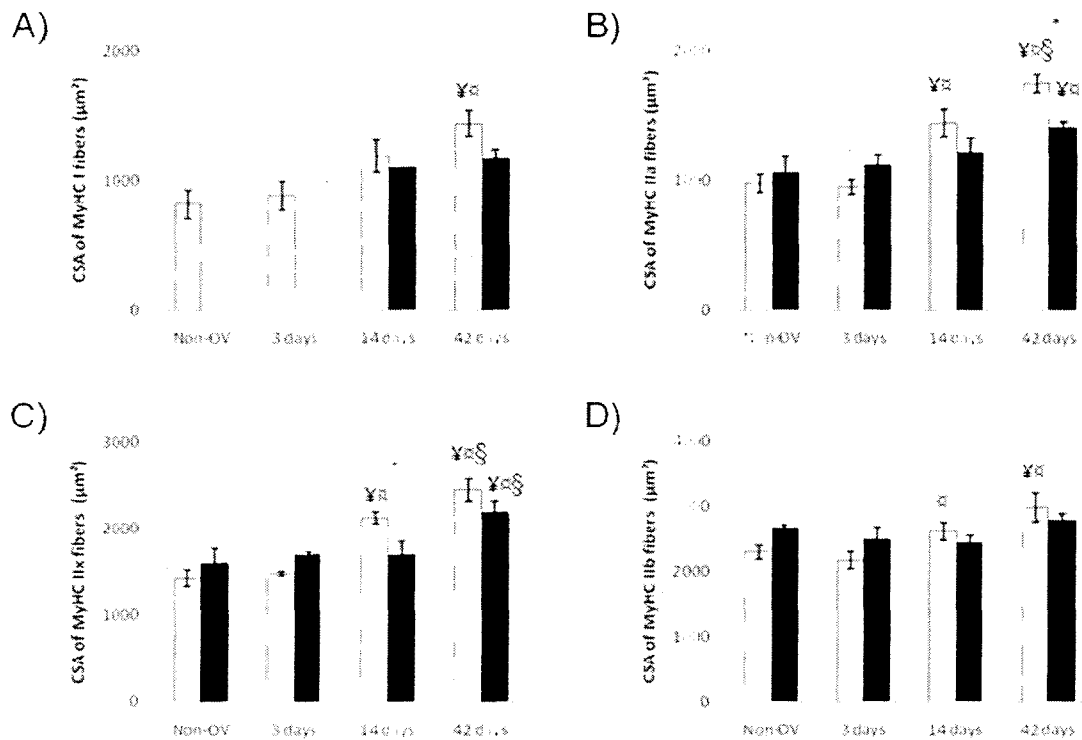


Figure 5 Cross-sectional area of muscle fibers according to major MyHC expression

Attenuation of fiber growth in *Mstn*^{-/-} mice (closed bars) of fibers expressing A) MyHC I, B) MyHC IIa, C) MyHC IIx, D) MyHC IIb compared to *Mstn*^{+/+} (open bars). Values for all graphs are means \pm S.E. n=4-7 per treatment group. * different (p<0.05) from wildtype (*Mstn*^{+/+}) counterpart, ¥ different (p<0.05) from non-overloaded control, ¤ different (p<0.05) from 3-day overloaded muscles, § different (p<0.05) from 2-week overloaded groups.

MyHC expression in response to overload

The statistical analysis of the overload-induced changes is presented in Table 2. In *Mstn*^{+/+} mice, a significant three-fold increase was found 2 weeks following surgery in the proportion of fibers expressing MyHC I (Fig. 6A). This proportion continued to increase over 7 times the initial level reaching 12%. *Mstn*^{-/-} mice did not show the same response as there was a blunting in fiber type remodeling and only one mouse had MyHC I fibers 2 weeks post-surgery. After 6 weeks, less than 1% of all fibers were expressing MyHC I. At each time point in *Mstn*^{-/-} mice, the proportion of fibers expressing MyHC IIa fibers was significantly lower than *Mstn*^{+/+} mice (Fig. 6B). Both

groups showed a slight increase in the expression of MyHC IIa, however, the difference was not statistically significant. We observed only a tendency towards a greater proportion of fibers expressing MyHC IIx in the *Mstn*^{-/-} group (14%; p=0.051) (Fig. 6C). *Mstn*^{-/-} mice had a larger proportion of fibers expressing MyHC IIb and this difference was maintained throughout the time-course (Fig. 6D). Additionally, a substantial and significant loss in the proportions of MyHC IIb fibers (44%; p<0.05) was also observed in wildtype (*Mstn*^{+/+}) animals only after 6 weeks. A different response was observed in *Mstn*^{-/-} mice where the proportion was maintained, however, statistical analysis did not reveal any significant interactions. From these observations, the decrease in fibers expressing IIb fibers in wildtype (*Mstn*^{+/+}) mice corresponded to a concomitant increase in cells displaying MyHC I. Despite the initial high levels of expression of fast isoforms of MyHC in *Mstn*^{-/-} muscles, these mice still maintained a capacity of the plantaris muscle to undergo the changes normally observed following functional overload. However, the response was blunted.

Table 2 Statistical analysis results of MyHC expression
p-values for the main effects and interactions of each variable. Asterisks denote significance (p<0.05)

Variable	KO effect	OV effect	Interaction
Proportion of fibers expressing:			
MyHC I	<0.001*	<0.001*	0.002*
MyHC IIa	<0.001*	0.120	0.504
MyHC IIx	0.768	0.017*	0.153
MyHC IIb	<0.001*	0.002*	0.335

Effects of overload on single fiber metabolic enzyme activity

The amount of each enzyme per unit cross-sectional area (OD unit / min · μm^2) of SDH and GPDH and total activities per cell (OD unit / min) were measured in control and 6 weeks overloaded mice (Fig. 7). There was a reduced amount of SDH activity per area (Fig. 7B) and total activity (Fig. 7C) in *Mstn*^{-/-} mice compared to *Mstn*^{+/+} mice, however, only the amount of SDH activity per area was found to be significantly lower than its wildtype (*Mstn*^{+/+}) counterpart. After 6 weeks of overload, the SDH rate per unit area was decreased non-significantly in *Mstn*^{+/+} but the total SDH rate was increased

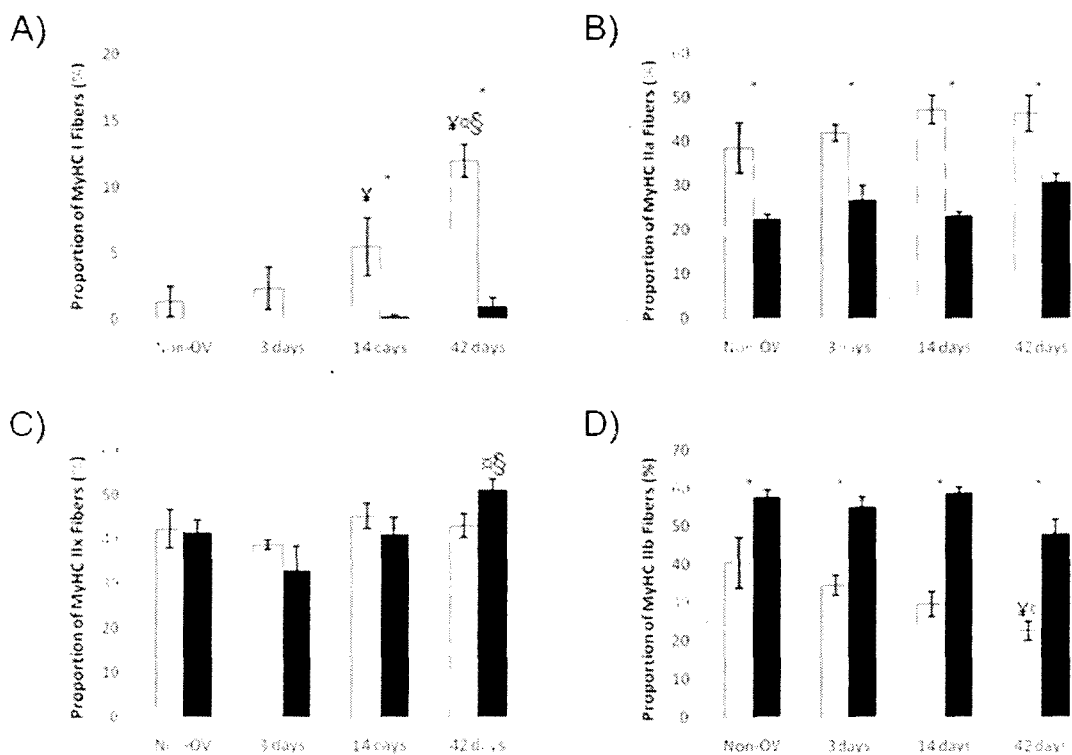
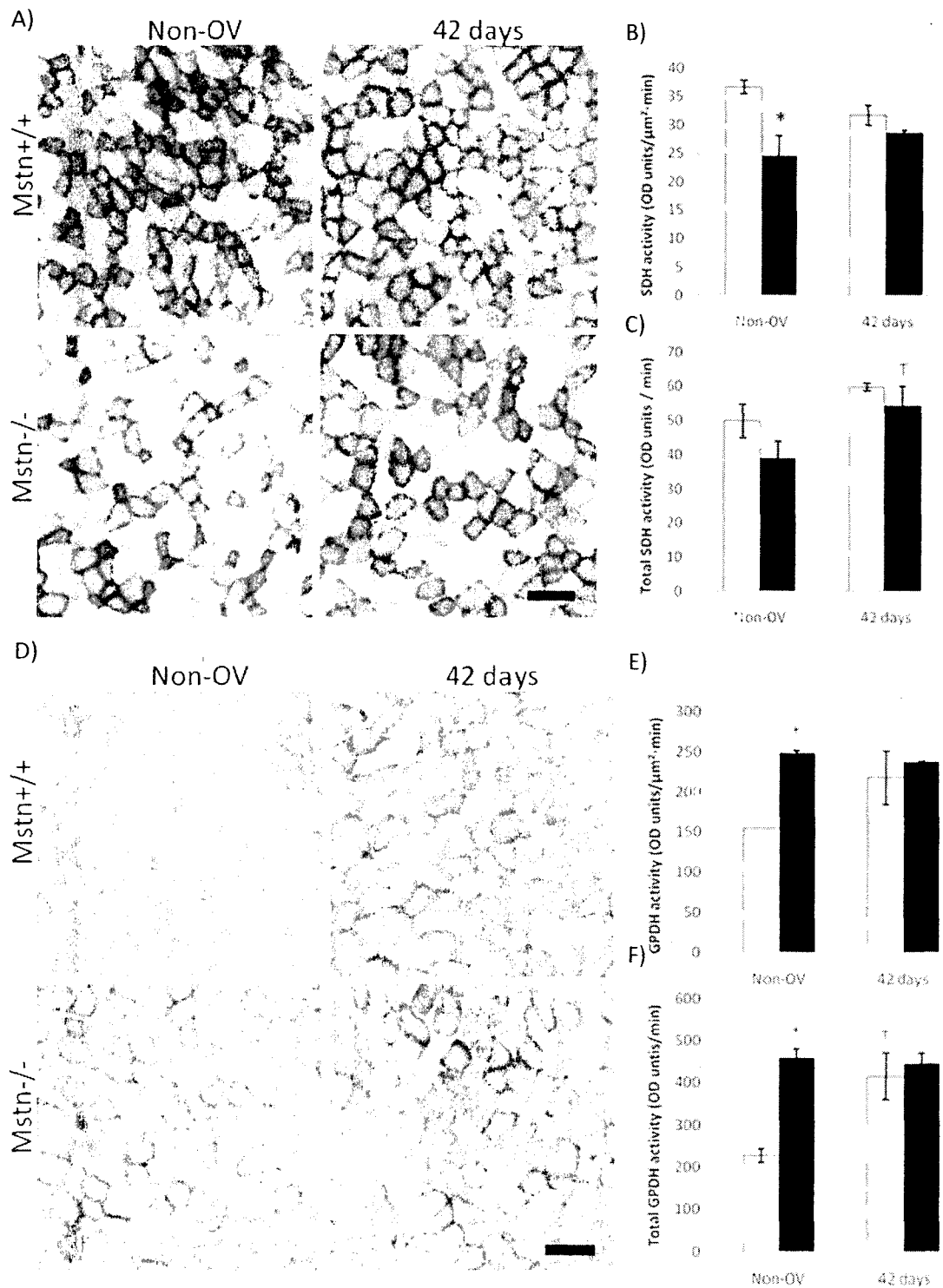


Figure 6 Changes in expression of major MyHC isoforms

Changes in the expression of myosin heavy chain isoforms display a blunting of transition from fast-to-slow as *Mstn*^{-/-} mice (closed bars) compared to their wildtype (*Mstn*^{+/+}) counterpart (open bars). Values for all graphs are means \pm S.E. n=4-7 per treatment group. * different (p<0.05) from wildtype (*Mstn*^{+/+}) counterpart, † different (p<0.05) from non-overloaded control, ‡ different from 3-day overloaded muscles, § different (p<0.05) from 2-week overloaded groups.



reflecting the larger cross-sectional area. The differences in the rates of activity in the *Mstn*^{+/+} mice were however not significant. On the other hand, in *Mstn*^{-/-} mice, the rate of SDH activity per area and the total SDH activity was greater following 6 weeks of overload. With respect to GPDH rates in non-OV *Mstn*^{-/-} muscle fibers, we observed 60% ($p < 0.05$) more activity per area and a doubling ($p < 0.05$) of total activity when compared to its wildtype (*Mstn*^{+/+}) counterpart. Following 6 weeks of overload, muscle fibers from *Mstn*^{+/+} animals showed an increase in GPDH activity per area and total activity with significant differences for the total activity. Fibers from *Mstn*^{-/-} mice maintained their GPDH activity.

Muscle damage and remodeling is more apparent in the distal portion of the plantaris

Previous literature of ablation surgery performed on *Mstn*^{+/+} rodents shows very little or no inflammation at the midbelly. However, in our case, *Mstn*^{-/-} mice display a very pronounced inflammatory response 3 days post-surgery marked by increased interstitial space, most likely due to edema and macrophage infiltration. When damage to muscle cells occurs, Evans blue dye (EBD) bound to albumin can enter those cells and the dye can be detected using a fluorescent microscope. Additionally, unspecific staining is detectable when staining only with a secondary Ig antibody. The unspecific staining found at the 3 day time point corresponded to labeling with EBD (data not shown). To further assess muscle damage after three days of overload, we obtained cross-sections of muscles stained with EBD at different levels in the belly of the muscle (Fig. 8A). As can be seen, only a very few cells are permeable to the dye in the

Mstn^{+/+} mice at the midbelly, whereas staining is visible in a good portion of cells in the whole midbelly of the *Mstn*^{-/-} muscle. At each level, *Mstn*^{-/-} mice consistently display a larger area of cells positive for EBD. The plantaris muscle is pennate and curiously, the uptake of EBD was mostly located in the belly region away from the tendon.

Additionally, longitudinal sections were obtained which confirmed our findings (Fig. 8B); following overload, both groups displayed damage in the distal portion of the muscle, however, the insult was greater in *Mstn*^{-/-} plantaris muscle.

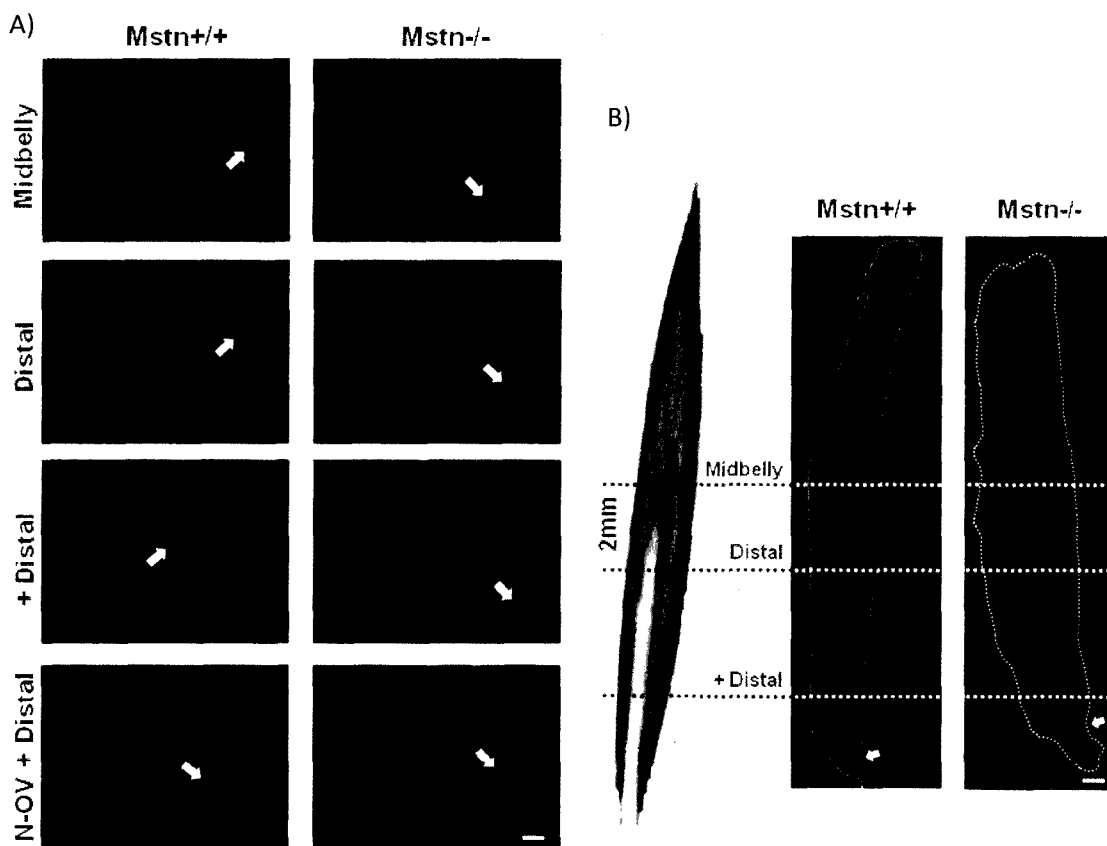


Figure 8 EBD uptake in 3-day overloaded muscles (Preliminary)

Representative images of the uptake of EBD in muscle overloaded for 3 days. EBD uptake shows more damage in the *Mstn*^{-/-} mice at A) midbelly, distal and +distal sections. +distal sections from non-overloaded mice were added as control to show absence of fluorescence in cells. n=2-3 per overload group; n=1 per control group. B) Longitudinal sections reveal extent of damage in the whole muscle. n=2 for *Mstn*^{+/+} group; n=1 for *Mstn*^{-/-} group. White arrows show location of distal tendon on cross-sections and longitudinal sections. Scale bar in A) 200 μ m and B) 500 μ m.

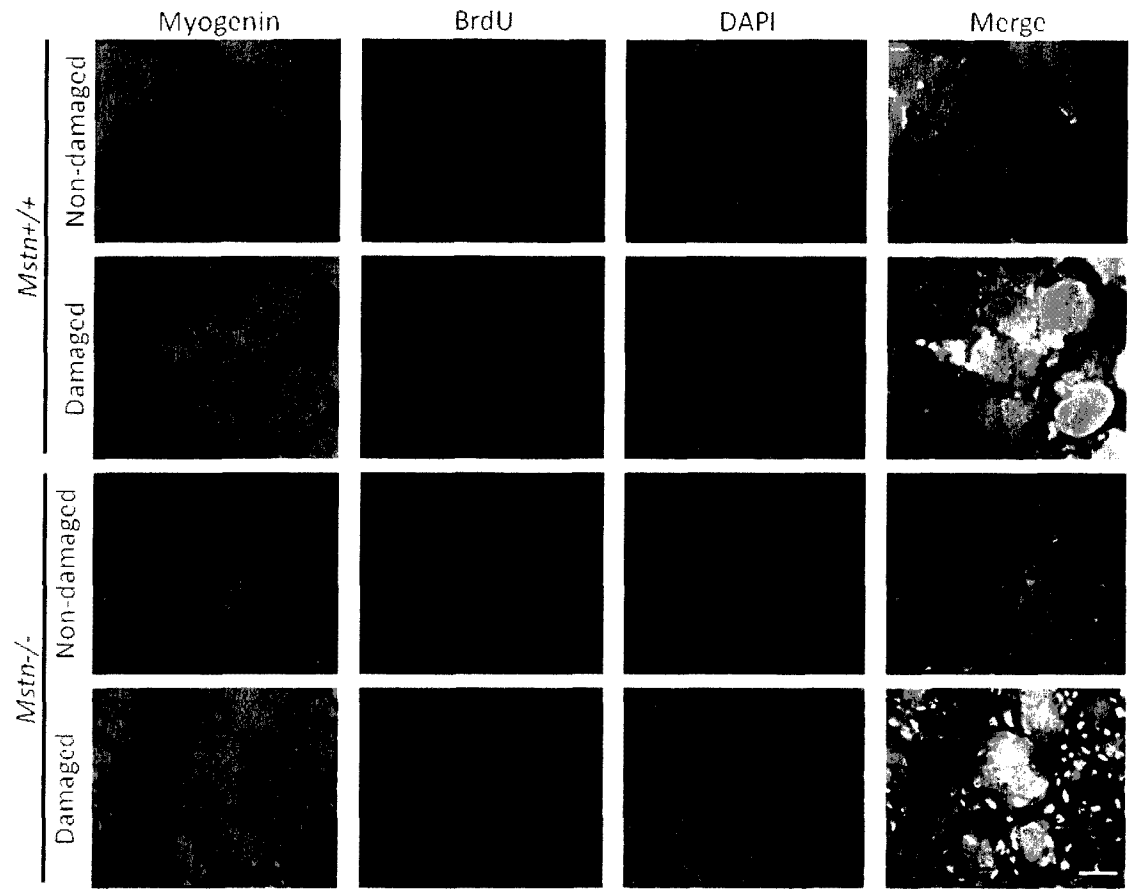


Figure 9 Immunofluorescent images of 1-week overloaded muscles (Preliminary)

Representative images of staining for myogenin (green), BrdU (red) and nuclei with DAPI (blue). Images from *Mstn*^{+/+} and *Mstn*^{-/-} muscles reveal a greater colocalization in areas with more damage. n=2 per wildtype(*Mstn*^{+/+}) group; n=1 per *Mstn*^{-/-} group.

The distal portion of the plantaris was also a region of major remodeling.

Immunofluorescence images from distal sections of plantaris muscles overloaded for one week are found in figure 9. In non-damaged areas of both groups, little or no BrdU was found indicating no regeneration in those regions. On the other hand, we observed a high concentration of nuclei colocalized with BrdU and myogenin in damaged areas. In the areas with larger interstitial space, many nuclei were found positive for BrdU, however, most were not expressing myogenin and were therefore not included in the analysis. Moreover, the one week time point corresponded to the appearance of cells

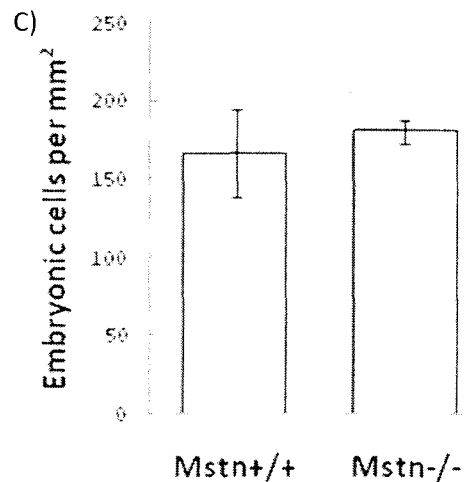
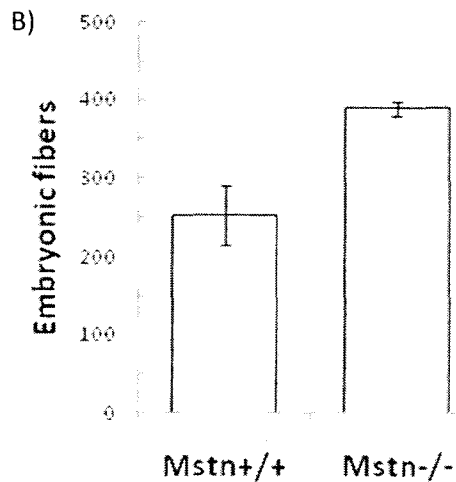
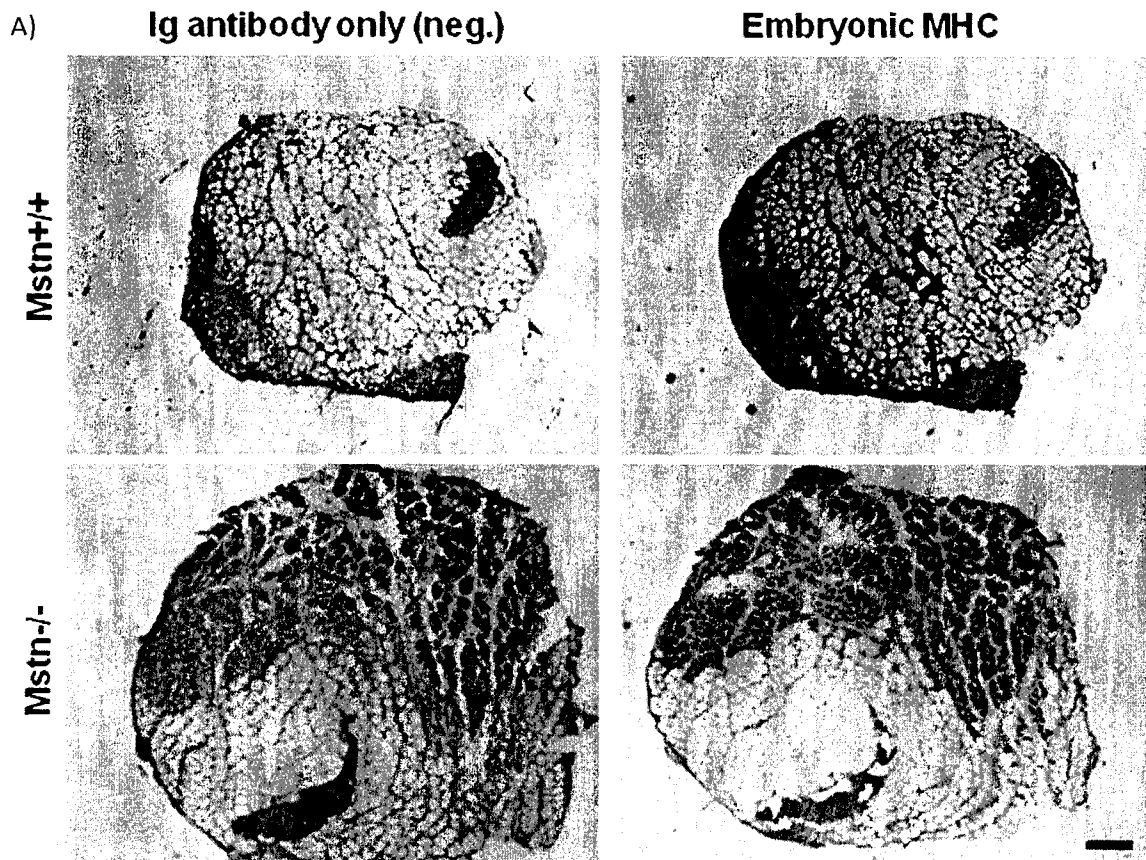


Figure 10 Embryonic cells after 1 week of overload

A) Representative images of staining for embryonic MyHC isoform. Image of unspecific staining was used to identify cells cells expressing the embryonic MyHC. B and C) Quantification of embryonic cells. Values for both graphs are means \pm S.E. n=4 per wildtype (*Mstn*+/+) group; n=2 per *Mstn*-/- group. Scale bar 200 μ m.

expressing embryonic MyHC (Fig. 10A). The count of embryonic cells (Fig. 10B) was greater in the *Mstn*^{-/-}, however, not significantly different. Additionally, no difference was found when normalizing the data to the distal belly area (Fig. 10C).

To find more evidence of hyperplasia, we analyzed distal sections stained with hematoxylin and eosin. Cells with central nucleation were already present after one week of overload (Fig. 11). One week post-surgery, major remodelling, marked by small centrally nucleated cells and many nuclei located interstitially can be observed. The large intact cells found in the muscles of *Mstn*^{-/-} plantaris muscles are mostly likely a result of remaining inflammation. After 2 weeks of overload, no more inflammation is seen. Both groups showed central nucleation, with some cells containing multiple nuclei. In fact, a few cells in *Mstn*^{-/-} muscles contained up to 6 nuclei. Muscles from those displayed more cells with at least one central nucleus (Fig. 11B), more nuclei located centrally (Fig. 11D) and a greater proportion of all cells were centrally nucleated (Fig. 11C), however, only the total number of centrally located nuclei showed a tendency for significance. To find out whether the muscles had returned to their pre-overloaded state, we stained and analyzed the muscles of mice overloaded for 6 weeks. To our surprise, centrally nucleated cells were still present (Fig. 11A & E-G). *Mstn*^{-/-} mice showed significantly more cells with at least one central nucleus, more nuclei located centrally, and a greater proportion of centrally nucleated cells than their wildtype counterparts.

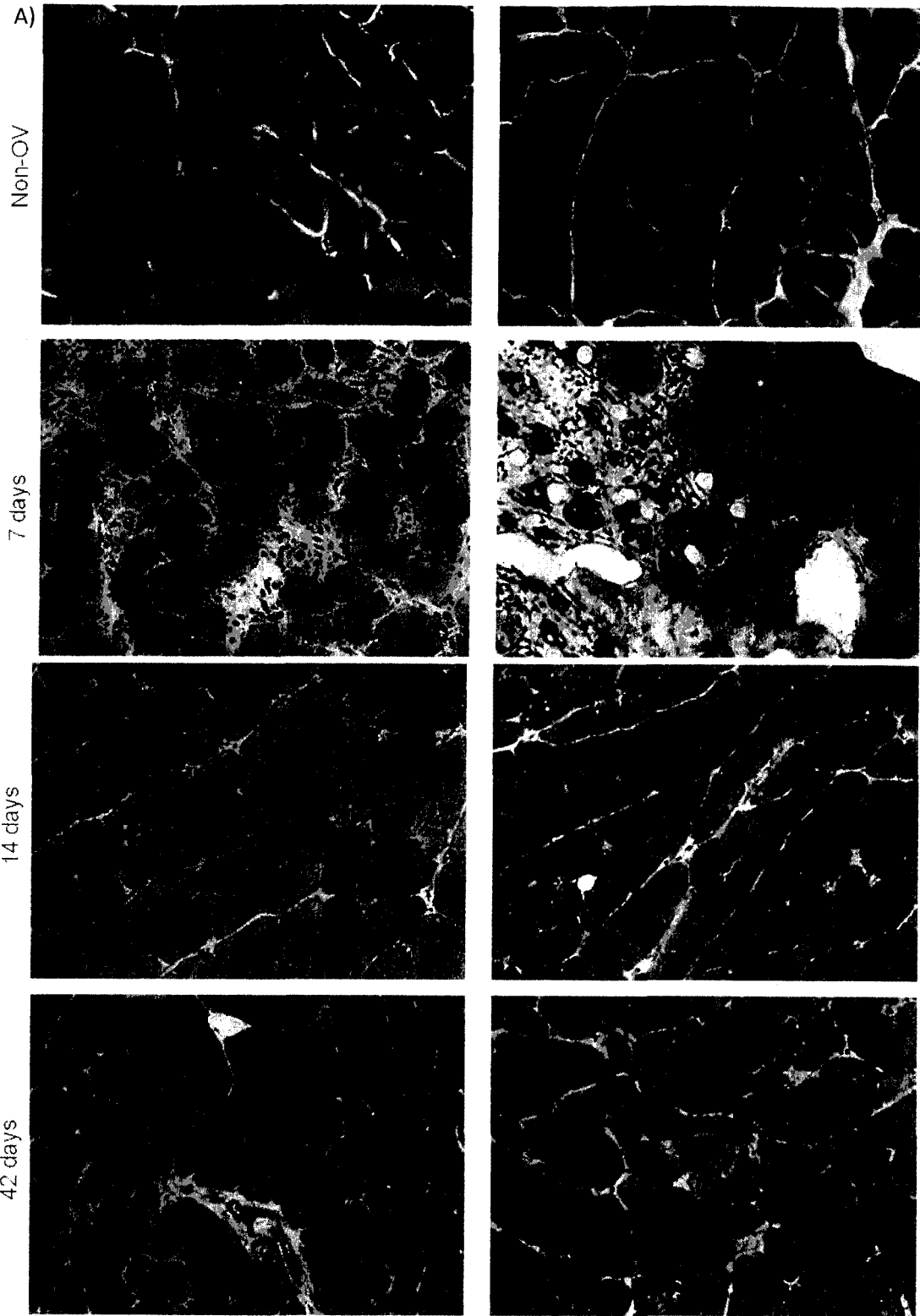


Figure 11 Central nucleation

A) Representative images of H&E in non-OV, 1-, 2- and 6-week overloaded muscles. Scale bar 50 μ m

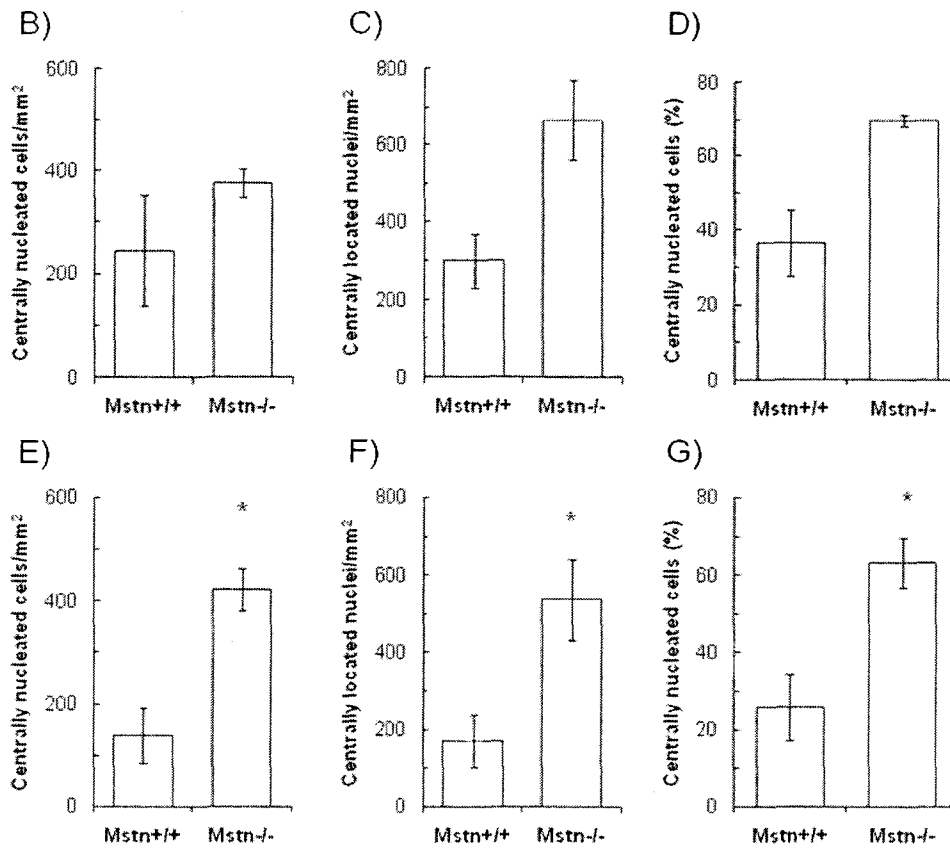


Figure 11 (cont'd)

Central nucleation after B-E) 2weeks and E-G) 6 weeks of overload. Values are means ± S.E. n=2-5 animals per treatment group. * different from wildtype (*Mstn*^{+/+}) group.

Western blots show activation of satellite cells

Protein levels of pax7, myoD and myogenin reflect activation of satellite cells (Fig. 12).

Under control conditions, pax7 protein levels are similar in wildtype (*Mstn*^{+/+}) and *Mstn*^{-/-} mice. Following the surgery, we observed an increase in pax7 protein levels in both groups (3.5 fold in both groups). In non-overloaded mice, a greater non-significant myoD level was observed (44%; $p > 0.05$) in *Mstn*^{-/-} mice. Following overload, myoD levels rise significantly after 1 day in *Mstn*^{+/+} mice (3.4 fold increase; $p < 0.05$). After 3 days, myoD in wildtype (*Mstn*^{+/+}) remained slightly elevated (2.3 fold), however, not significantly different from its non-overloaded control. In *Mstn*^{-/-} mice, myoD protein

levels were elevated only at 1 day post-OV (2.8 fold), after which they return to its control value.

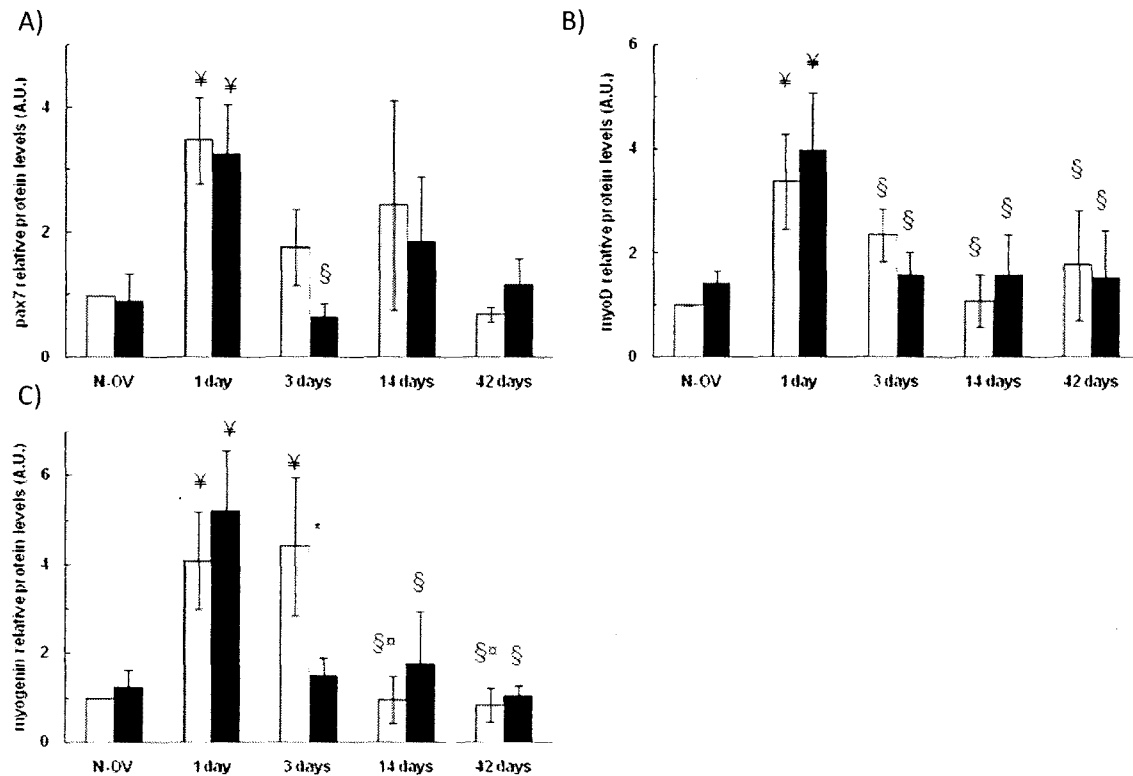


Figure 12 Pax7, myoD and myogenin relative protein levels

Quantification of A) pax7 B) myoD and C) myogenin protein levels in *Mstn*^{+/+} (open bars) and *Mstn*^{-/-} (closed bars). Values are relative to the *Mstn*^{+/+} non-overloaded control. Values are means \pm S.E. n=2-3 per treatment group. * different from respective *Mstn*^{+/+} ($p < 0.05$). † Different from non-overloaded control ($p < 0.05$). § Different from 1 day overloaded ($p < 0.05$). ¶ Different from 3 day overloaded ($p < 0.05$).

As for myogenin, a different pattern of expression was observed, however, no significant interactions were found. In the control group, no significant difference was found in the protein level (23% higher, $p > 0.05$). After 1 day, myogenin levels were significantly higher in *Mstn*^{+/+} mice (4.1 fold; $p < 0.05$) and remained elevated up to 3 days following overload (4.4 fold; $p < 0.05$). Interestingly, myogenin protein levels increase after 1 day (4.2 fold; $p < 0.05$), but return to their non-overloaded level after 3 days. These data show that satellite cells are activated and have committed to the myogenic lineage.

Discussion

We used the functional overload model to examine differences in the growth response between *Mstn*^{-/-} and *Mstn*^{+/+} mice. Contrary to our hypothesis, the growth in *Mstn*^{-/-} mice was not potentiated but in fact blunted. With the exception of absolute muscle mass and cross-sectional size of IIB fibers, all variables measuring size show a significant or a tendency ($P < 0.06$) towards a significant interaction where the muscles of *Mstn*^{-/-} mice did not grow to the same extent as their wildtype (*Mstn*^{-/-}) counterparts. Following 2 and 6 week of overload, the cross-sectional area of muscle fibers of all individual fiber types from *Mstn*^{+/+} mice exceeded that of *Mstn*^{-/-} mice. On the other hand, the overall cross-sectional area of fibers irrespective of their MyHC type was still greater in *Mstn*^{-/-} compared to wildtype (*Mstn*^{+/+}) counterparts. This could be explained by the greater proportion of the larger MHC IIB fibers in *Mstn*^{-/-}. The proportion of those larger fibers was also maintained after 2 and 6 weeks in *Mstn*^{-/-}. In non-overloaded animals, the absence of myostatin leads to significant muscle size, however, the improved strength is not proportional to the greater muscle mass [154]. This could partially explain the lack of growth seen in our *Mstn*^{-/-} mice following overload suggesting the plantaris muscle was not stressed enough to induce growth. Recent evidence suggests endurance exercise alone does not induce hypertrophy, but rather a switch towards a more oxidative phenotype [102, 103]. In those studies, muscle fiber size was maintained or slightly reduced following endurance exercise suggesting hypertrophy is a result of the increased load on the plantaris muscles rather than a response to exercise. Another possible explanation could be that these mice might have

potentially reached their maximal size. This is highly unlikely, since targeting other ligands in addition to myostatin quadruples muscle mass in mice[155]. Our results then suggest that other pathways are able to compensate for the lack of myostatin, namely activin or follistatin.

We replicated previous results showing a greater proportion of fibers expressing MyHC IIb[137, 156]. We also displayed a blunted capacity for *Mstn*^{-/-} to adapt to increased load which concords with previous findings[102, 103]. The absence of fibers expressing MyHC IIb could stem from a reduced fatigue-resistance to exercise[102], however, our data (not shown) supports similar levels of daily volunteer running. This would suggest myostatin would be important in the expression of slow MyHC isoforms. Interestingly, myostatin is found more abundantly in fast muscles[157]. Calcineurin is an important regulator of the fast to slow fiber conversions that occur during overload[135].

Myostatin could act in cooperation with calcineurin in fiber type remodeling[158, 159].

In agreement with previous reports, we found lower SDH activity in *Mstn*^{-/-} mice which also matches the absence of the fibers expressing the MyHC I isoform[160]. To further characterize the capacity of skeletal muscles in *Mstn*^{-/-} mice to adapt to the functional demands of overload, we assessed SDH and GPDH activity. Endurance exercise induced an increase in SDH activity in both *Mstn*^{-/-} and wildtype (*Mstn*^{+/+}) mice. Strangely, functional overload led to a greater increase of SDH activity in *Mstn*^{-/-} mice. The increase in oxidative capacity did not concord with the blunted response in the different MyHC isoforms. Moreover, the final SDH activities were similar in both groups. This

would suggest a great capacity of muscle fibers to adapt to increased demands irrespective of the contractile properties of their MyHC isoforms. On the other hand, as expected, GPDH activity was significantly higher in *Mstn*^{-/-} control mice. Additionally, the increase in GPDH activity in *Mstn*^{+/+} mice matched previous findings from our laboratory[136]. Overloaded *Mstn*^{-/-} muscles maintained their GPDH activity and final levels were similar to the wildtype (*Mstn*^{+/+}) group. Possibly, muscles from *Mstn*^{-/-} mice could retain their levels of GPDH activity since they do not follow the traditional fiber remodeling towards slower, more energy efficient phenotypes. GPDH activity would reflect the load requirements and not the muscle recruitment frequency.

The uptake of EBD clearly shows more damage in overloaded *Mstn*^{-/-} muscles. To explain the greater damage found in *Mstn*^{-/-} mice, myostatin increases the expression of collagen genes and promotes collagen formation[161, 162]. Myostatin-deficient mice also have smaller and brittle tendons making the tendons more susceptible to damage[163]. This aspect becomes particularly important for the populations that might benefit from treatment through the inhibition of the myostatin pathway. Elderly people have altered tendon mechanical properties[164], and if myostatin is required for collagen expression, such a therapy could be devastating. With training, tendon mechanical properties such as cross-sectional area, length and stiffness can be improved[165, 166]. Since disuse can lead to the opposite effect[166], it would be interesting to see whether the reduced collagen expression is a result of the genetic mutation or a consequence of abnormally large muscles not used to their full extent. Another explanation for the greater damage includes a greater angle of pennation

leading to differences in the biomechanical force transmission through the muscle fiber. Interestingly, myostatin is located at the myotendinous junctions possibly providing protective effects[167]. Body weight could also play a factor, however, *Mstn*^{+/+} mice with similar body weights to *Mstn*^{-/-} mice were overloaded and the *Mstn*^{-/-} mice still displayed more muscle damage (data not shown). Whether damage is necessary for remodeling is still uncertain. Intuitively, more damaged areas would trigger more regeneration and our findings support this idea.

Inflammation is an important process in early regeneration which facilitates myogenesis via phagocytosis of cellular debris and the release of growth factors[141, 168-170].

Ibuprofen, a non-steroidal anti-inflammatory and analgesic drug, is a selective inhibitor of the cyclooxygenase (COX) pathway[171] involved in skeletal muscle regeneration[172]. The treatment with COX inhibitors does not affect the weight of non-injured muscles[172], and therefore, our control non-overloaded animals were not given any ibuprofen. Since it is not involved in muscle damage, it would not affect the absorption of EBD in overloaded muscles. Additionally, daily treatment with COX inhibitors can block skeletal muscle hypertrophy induced by functional overload[173]. In our study, ibuprofen was removed after 3 days when no differences in macrophage accumulation have been previously observed[173].

Since the plantaris muscle of *Mstn*^{-/-} mice did not grow as much as those of their wildtype counterparts (*Mstn*^{+/+}) after 2 and 6 weeks of overload, we looked at earlier time points to determine satellite cell activation. Previous studies have shown an

upregulation in myogenic markers after just 1 day and started to decline only after 7 days[174]. Distally, more nuclei were labeled with BrdU and more labeled nuclei colocalized with myogenin. Our findings concur with previous findings observing myogenin localized in the nuclei after 7 days of overload[175, 176]. The same group also found myoD and myogenin to be expressed before PCNA, an indicator of proliferation, could be observed. The early expression of those MRFs suggests that a first wave of myogenic precursor cells can differentiate into myotubes without proliferating. If more extensive damage occurs, the remaining satellite cells can divide to provide the necessary cells to complete the regeneration. The regions surrounding the damage were filled with cells staining for the embryonic isoform of myosin indicating new cell formation. Despite the greater number of cells expressing embryonic MyHC, the value normalized to the belly area revealed no difference from control. More damaged areas were found in the overloaded muscles of *Mstn*^{-/-} mice and therefore secondary binding could potentially hide some embryonic cells. Additionally, one of our wildtype mice (*Mstn*^{+/+}) showed more embryonic cells than its *Mstn*^{-/-} counterpart, suggesting a great amount of variability in the response. Moreover, larger areas of fiber regeneration were found in the muscles overloaded for 1 week in *Mstn*^{-/-} animals.

An analogy to muscle regeneration can be made with the mdx mouse. The mdx mouse, a genetic ortholog of Duchenne and Becker muscular dystrophies, provides a model system for repetitive muscle degeneration and regeneration. In the mdx mouse, a mutation in the gene for dystrophin results in absence of the protein from the sarcolemma and muscle fiber necrosis[177]. Satellite cells are involved in the

regeneration of muscles affected by muscular dystrophy; however, the progressive degeneration leads to a decrease in satellite cell number and proliferative potential[178]. Beneficial effects from myostatin absence or blockade have been reported possibly due to increased proliferation of satellite cells[10, 179].

The requirement for satellite cell activity in muscle hypertrophy is still debated[57, 60, 176, 180]. Most studies opposing the addition of new cells looked at the role of the Akt pathway in muscle growth. On the other hand, studies using the functional overload model support the idea of hyperplasia. The most convincing evidence supporting hyperplasia comes from studies using irradiation to suppress the mitotic capability of satellite cells. Since mature skeletal muscle fibers are post-mitotic, lack of growth following overload clearly demonstrates the importance of satellite cells in hypertrophy [58, 180, 181]. To further support the requirement of satellite cells for hypertrophy, inhibition of satellite cell activation has also blocked overload-induced growth[182]. Following overload, muscle mass can double within 2-4 weeks, however, in our lab, proliferation of satellite cells has not been found to be a major contributor to the rapid growth[91]. Most recently, a contradicting study involving myostatin signaling refuted hyperplasia as a major contributor to the larger muscle mass observed in *Mstn*^{-/-} mice[51]. The authors of the study used lower concentrations of myostatin to inhibit satellite cell proliferation. Additionally, they used aged mdx animals to demonstrate that myostatin absence does not rescue the dystrophic phenotype. Therefore, we still believe that myostatin is still involved in satellite cell activation and proliferation. Our findings of satellite cell activity might explain why little evidence has been found of

newly formed cells in the midbelly region of overloaded muscles. *In vitro*, lack of myostatin in the differentiation medium delays the differentiation process and would therefore allow to prolong the proliferation of myoblasts[49]. Closer to the myotendinous junction, after one week, the appearance of cells expressing the embryonic isoform of MyHC, followed by central nucleation after 2 weeks of overload provide some evidence of hyperplasia. Supporting this idea, in *Mstn*^{-/-} mice, we observed a greater number of centrally nucleated cells per mm² and a greater number of nuclei located centrally at the distal ends of the plantaris muscle after 2 and 6 weeks of overload. Despite the lack of significance between the groups at 2 weeks, combining results at the midbelly and distal sections would most likely show a greater propensity for *Mstn*^{-/-} muscles to grow through hyperplasia. Moreover, no differences in the estimated cell count were observed at the midbelly area after 6 weeks suggesting an important role for growth in the distal portion of the muscle. Our data obtained at the midbelly of muscle mass, cross sectional area and proportions match previous findings. Thus changes observed at the midbelly do not reflect the remodelling in the distal portion of the muscle. In light of the regeneration occurring in the distal portion of the plantaris muscle, further characterization is necessary to assess the changes associated with functional overload.

The IGF/Akt pathway might also be involved in the hypertrophic response resulting from functional overload. However, some studies suggest a limited role. By inhibiting IGF, hypertrophy was not blocked following synergist ablation[55]. Although IGF and Akt can induce hypertrophy *in vivo*, they have a limited role in satellite cell activation[60, 183].

To further support this, irradiated muscles still grow when treated with IGF-I although to a lesser extent[57]. This suggests the IGF-I pathway induces hypertrophy through increased protein synthesis.

Moreover, our preliminary western blots did not show any differences between *Mstn*^{+/+} and *Mstn*^{-/-} mice. Our results showed a peak in the regulatory proteins after 1 day of overload, and returning to basal levels after 3 days, earlier than previously found[87]. Differences among species could explain the differences in the response. Myogenin levels were maintained up to 3 days in wildtype mice; however, the difference was not significant. If proliferation only begins after 3 days marked by an upregulation of PCNA[174], a second peak could be seen at later time points explaining the presence of myogenin in the nuclei found with our immunofluorescence.

Our study not only shows hyperplasia as a major contributor to growth in *Mstn*^{-/-} mice, but it also calls us to revisit the current notion about muscle growth in general.

Acknowledgements

I thank Mathieu St-Louis for all the work done on the immunofluorescence, the Western blots and for useful discussions; Mohommad Al-Khalaf for the technical support at the initial stages of the project.

Chapter 3: Absence of myostatin does not protect skeletal muscles from atrophy induced by denervation

Manuscript in preliminary phase of preparation

Abstract

Myostatin is a member of the TGF- β family of growth factors and a negative regulator of muscle mass. Myostatin has been proposed a therapeutic agent to prevent atrophy. To investigate the role for Mstn in muscle fiber atrophy, we compared the effects of denervation in Mstn Knockout (*Mstn*^{-/-}) and wildtype (*Mstn*^{+/+}) mice. Two weeks of denervation led to significant and comparable loss in muscle mass of the soleus and plantaris of the wildtype (*Mstn*^{+/+}) and *Mstn*^{-/-} mice. The comparably lower mass was concomitant with reduction of the cross-sectional area of individual fibers in the plantaris and soleus muscle in both sets of mice. During the same time frame, no significant changes in myosin heavy chain type profiles of *Mstn*^{+/+} and *Mstn*^{-/-} muscles were found. This study shows no sparing effect of the absence of myostatin during skeletal muscle atrophy following denervation suggesting an alternative pathway for nerve-mediated atrophy. Funded by CIHR, NSERC and CRC.

Introduction

Muscle atrophy in animal models is regulated in response to changes in workload, activity and in the presence of pathological conditions [66, 184]. Muscle degeneration may lead to a debilitating condition which is often seen in disuse, aging, and muscular dystrophy. Despite the importance and impact of losing muscle mass, the mechanisms leading to atrophy are still poorly understood. The same biochemical and chemical changes are believed to occur in muscles during the various types of atrophy [185]. Myostatin, an important regulator of skeletal muscle mass, is increased in many different models of atrophy[78-81]. Myostatin is expressed in skeletal muscle and in heart[2, 186]. Once synthesized, myostatin is processed and secreted into the blood stream[2, 16].

Myostatin inhibition, for instance via the administration of antibodies against this protein, has been proposed as a method to limit muscle atrophy after paralysis since the disruption of its gene expression leads to dramatic increases of skeletal muscle mass[2]. Loss of myostatin results in a combined effect of muscle fiber hypertrophy and hyperplasia[2]. Myostatin loss in dystrophic mice through its inhibition by injection or gene deletion results in increased muscle mass and muscle strength[12]. Also, removal of myostatin improves the sarcopenic phenotype [13]. To date, the only studies looking at the rescuing effects of skeletal muscle atrophy have used glucocorticoid administration or hindlimb unloading to induce muscle atrophy[187, 188]. Denervation requires the removal of a portion of a nerve which leads to complete loss of neural input and muscle activity. Atrophy varies greatly due to the function of the

different muscles (weight bearing versus non-weight bearing; fast versus slow). Changes in the expression of the different isoforms of MyHCs are also observed following denervation[106, 114]. The direction of the change depends on the predominant fiber type of the muscle prior to denervation[106, 115]. Fast muscles develop a tendency towards a slower phenotype and slow muscle show a shift towards a faster phenotype. Additionally, many genes are differentially expressed during denervation. MuRF1 and MAFbx are among the mRNA most drastically induced by denervation[66, 109, 110]. The expression of those genes is dependent on the FoxO family of transcription factors, FoxO1 and FoxO3a[74, 109, 111].

Myostatin knockout has led to amelioration in muscle phenotype after injection of glucocorticoids[187]. However, the myostatin knockout muscles were not spared from atrophy when subjected to gravitational unloading[188]. Therefore, in our study, we set to assess the effects of denervation-induced atrophy on weight bearing muscles when myostatin is not present.

Materials and methods

Animal care and protocols

All animal care and experimental procedures were performed in accordance with the guidelines established by the Canadian Council of Animal Care. These procedures were approved by the University Animal Research Ethics Committee (UAREC) of Concordia University. *Mstn*^{-/-} mice were kindly donated by Dr. S.-J. Lee. (Johns Hopkins University School of Medicine, Baltimore, MD)

Animal surgeries

All surgical procedures were performed under aseptic conditions on animals anesthetized by intramuscular injection (1.2 µl/g) of 100 mg/ml ketamine hydrochloride and 10 mg/ml xylazine in a volume ratio of 1.6:1. Under sterile conditions, the sciatic nerve was exposed at the level of the sciatic notch. A segment of 4-5 mm of the sciatic nerve was excised just below the sciatic notch. The contralateral limb was left untouched. Additionally, non-operated mice were used as control. The mice were kept denervated for 3, 7 or 14 days. To ensure full denervation, neurological tests were performed as described previously[189]. Following the treatment period, the animals were deeply anesthetized again and the soleus, plantaris, gastrocnemius, plantaris and tibialis anterior were excised, embedded in OCT (Tissue-Tek, Torrance, CA) and frozen in melting isopentane before being put in liquid nitrogen. Tissues were stored at -86°C until processed.

Immunohistochemistry

Antibodies used were as follows: MyHC I : A4.840, Developmental study hybridoma bank (DSHB, University of Iowa, Iowa city, IA); MyHC IIa : SC71 (DSHB); MyHC IIx : 6H1 (DSHB); MyHC IIb : BF-F3 (DSHB); anti-mouse HRP : IgG A8924 (Sigma-Aldrich) or IgM A8786 (Sigma-Aldrich). To determine the MyHC isoform expressed by each fiber, cryosections (10 μ m) were cut from the same anatomical location in each muscle midbelly and recovered onto Superfrost[®] Plus microscope slides (Fisher Scientific). First, the sections were blocked in 5% goat serum in a carrier solution consisting of 0.5% bovine serum albumin (BSA) in 25 mM PBS (pH = 7.4) for 30 minutes. The sections were then probed overnight at 4°C in carrier solution with one of the following primary antibodies raised against the different MyHC types (I 1:25; IIa 1:12.5; IIx undiluted; IIb 1:25). After three 10-min PBS rinses, sections were then probed at room temperature with either horseradish peroxidase-conjugated anti-mouse IgG (MyHC type IIa 1:25) or IgM (MyHC type I, IIx, IIb). The sections were rinsed three times with PBS for 10 minutes. The bound antibody complexes were then visualized using DAB as per the manufacturer's instructions. DAB makes the bound peroxidase-conjugated antibodies turn brown and can be visualized with a light microscope.

Three to four distinct regions were selected randomly from the midbelly of each plantaris and soleus muscle. All fibers in those regions were identified across each serial tissue section with the aid of a Retiga SRV camera (QImaging, Surrey, BC, Canada) mounted on an Olympus BX-60 (Olympus, Center Valley, PA) microscope. Each area of interest comprised approximately 75 fibers. The images were analyzed using ImagePro

Plus version 6.2 software (Olympus). Fibers were classified according to their staining profile with the distinct antibodies. For consistency, cell size was measured on a single non-stained muscle section fixed with 1% paraformaldehyde for 20 minutes in PBS followed by 3 washes in PBS for 5 minutes each.

Protein extraction and immunoblotting

The antibodies used were: Myostatin : AB3239, 1:750 (Millipore, Bedford, MA); alpha tubulin : 2125, 1:2000 (Cell Signaling Technology); anti-rabbit HRP : 7074, 1:2000 (Cell Signaling Technology). Muscles were homogenized in RIPA buffer [PBS (pH 7.4), 1% Igepal, 0,5% Sodium deoxycholate, 0,1% SDS, 10 µg/ml leupeptin, 10 µg/ml aprotinin, 1 mM 4-(2-aminoethyl)benzene sulfonyl fluoride, 10 mM NaF, and 1 mM sodium ortho vanadate] using a TissueTearor homogenizer (ColeParmer, Montreal, QC) at low speed for 45 seconds. Homogenates were centrifuged at 13 000 x g for 30 min at 4 C to pellet cell debris. The supernatant was quantified using the QuickStart Bradford dye reagent (Bio-Rad, Mississauga, Ontario, Canada). For protein analysis, 150 µg protein were resolved by SDS-PAG, transferred to a PVDF membrane (Millipore). The protein/antibody complex was revealed by chemiluminescence using the Immobilon Western kit (Millipore).

Statistical analysis

The data was tested for homogeneity of variance, and in the case where homogeneity was found, a two-way ANOVA was used. LSD was used as a *post hoc* test when appropriate. When the variance between the groups was not homogenous, the Kruskal-Wallis test was performed. The statistics were done with computer assistance using SPSS Statistics GradPack version 17.0.

Results

Myostatin protein is found in muscles and serum

To confirm the presence of myostatin protein, we immunoblotted 150µg of protein from skeletal muscle, heart and blood serum of wildtype (*Mstn*^{+/+}) mice (Fig. 13). We used the *Mstn*^{-/-} mouse as a control for the antibody. The data show that myostatin protein is easily detected as the precursor form in skeletal muscle of wildtype (*Mstn*^{+/+}) mice. A very faint band at 13kDa can be seen in the skeletal muscle of *Mstn*^{+/+} mice. Since active myostatin is secreted into the blood stream, only the active portion (13kDa) is visible in plasma of *Mstn*^{+/+} mice. Myostatin was, however, not detectable in the heart. The absence of bands at the corresponding height of 13 and 55kDa in the lanes containing *Mstn*^{-/-} samples confirms the specificity of the myostatin antibody.

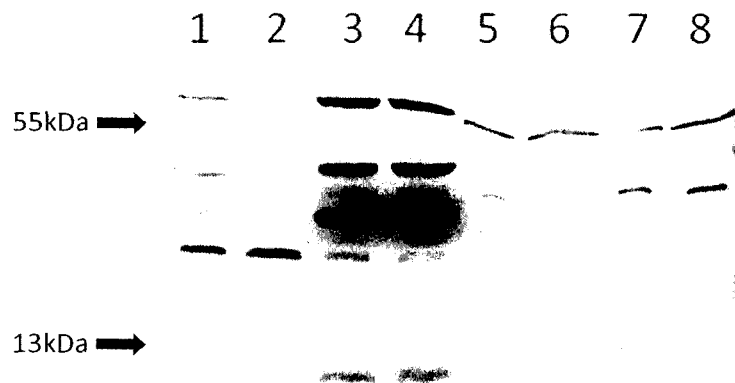


Figure 13 Myostatin protein in skeletal muscle, heart and blood serum (Preliminary)

Western blot for myostatin protein in skeletal muscle (lanes 1&2), heart (lanes 3&4) and blood serum (lanes 5-8). Myostatin is present in *Mstn*^{+/+} mice (lanes 1,3,5,6) and absent in *Mstn*^{-/-} mice (lanes 2,4,7,8). Myostatin is detected as the precursor protein in skeletal muscle and as the active protein in blood serum. Myostatin was not found at detectable levels in the heart. Quantity loaded: 150µg in each lane. n=1 for skeletal muscle and heart; n=2 for serum

Muscle mass loss is not different in Mstn^{-/-} mice

Absolute muscle mass is displayed in Figure 14 (A-C). Additionally, to control for the difference in body weight, we divided the absolute muscle weight by the animal's body weight to obtain the relative muscle mass (Fig. 14D-F). A significant denervation effect was observed in all weight bearing muscles of both wildtype (*Mstn^{+/+}*) and *Mstn^{-/-}* mice. In *Mstn^{+/+}* mice, denervation induced a significant reduction in absolute and relative muscle mass of 25 to 40% in the soleus, plantaris and gastrocnemius muscles. Similar results were observed in the *Mstn^{-/-}* muscles. These data show no sparing effect of muscle mass in the absence of myostatin.

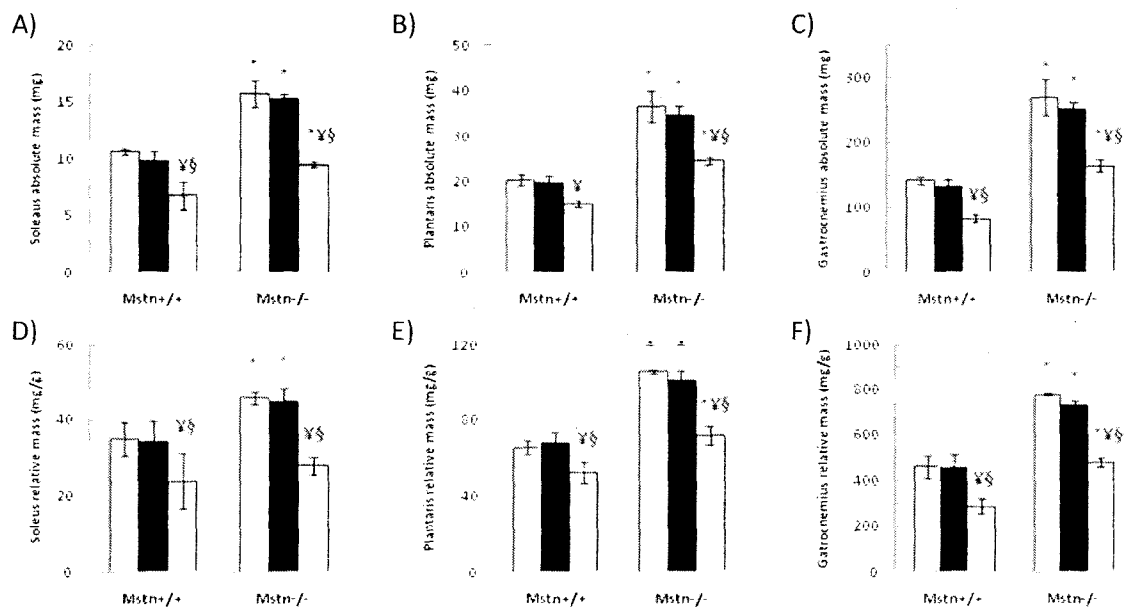


Figure 14 Muscle weights

Absolute (A-C) and relative (D-F) muscle mass of soleus (A,D), plantaris (B,E) and gastrocnemius (C,F). Open bars: Non-denervated controls; black bars: Contralateral limb to denervated side; gray bars: Denervated limb. Values are means \pm S.E. n=3-4 per treatment group. * Different from wildtype (*Mstn^{+/+}*) ($p < 0.05$); § Different from non-denervated control ($p < 0.05$); ¥ Different from contralateral limb ($p < 0.05$).

Changes in CSA are similar in $Mstn^{+/+}$ and $Mstn^{-/-}$ mice

We used fiber CSA as another measure of atrophy (Fig. 15). In plantaris, fibers expressing the different MyHC isoforms displayed different sensitivities with respect to size in response to denervation (Fig. 15A). More specifically, only fibers expressing MyHC IIb showed atrophy compared to fibers in the contralateral limb and the non-denervated muscles. The size difference was similar in wildtype ($Mstn^{+/+}$) and $Mstn^{-/-}$ mice. No difference in size was apparent in fibers expressing other MyHC isoforms. In contrast to the plantaris, with the exception of MyHC IIb fibers, all myofibers displayed a smaller CSA following denervation (Fig. 15B). The changes in CSA in both wildtype ($Mstn^{+/+}$) and $Mstn^{-/-}$ mice correspond to the muscle mass lost in the soleus.

Expression of MyHC isoforms

We assessed changes in the expression of the major isoforms of MyHC in plantaris and soleus muscle fibers after 14 days of denervation (Fig. 16). In order to eliminate discrepancies due to the coexpression of different isoforms of MyHC in a single fiber, the proportion of the fibers were pooled into their major isoforms. Detectable changes in plantaris major MyHC profiles were not apparent after 14 days of denervation in both groups (Fig. 16A). In contrast to the plantaris, subtle transitions in $Mstn^{+/+}$ mice in adult MyHC expression were observed within this same time frame under certain conditions in the soleus, such that the IIa MyHC isoform was expressed in a greater proportion of cells, whereas some cells were no longer expressing MyHC I (Fig. 16B). In $Mstn^{-/-}$ mice, changes in MyHC expression were prevented in the denervated limb.

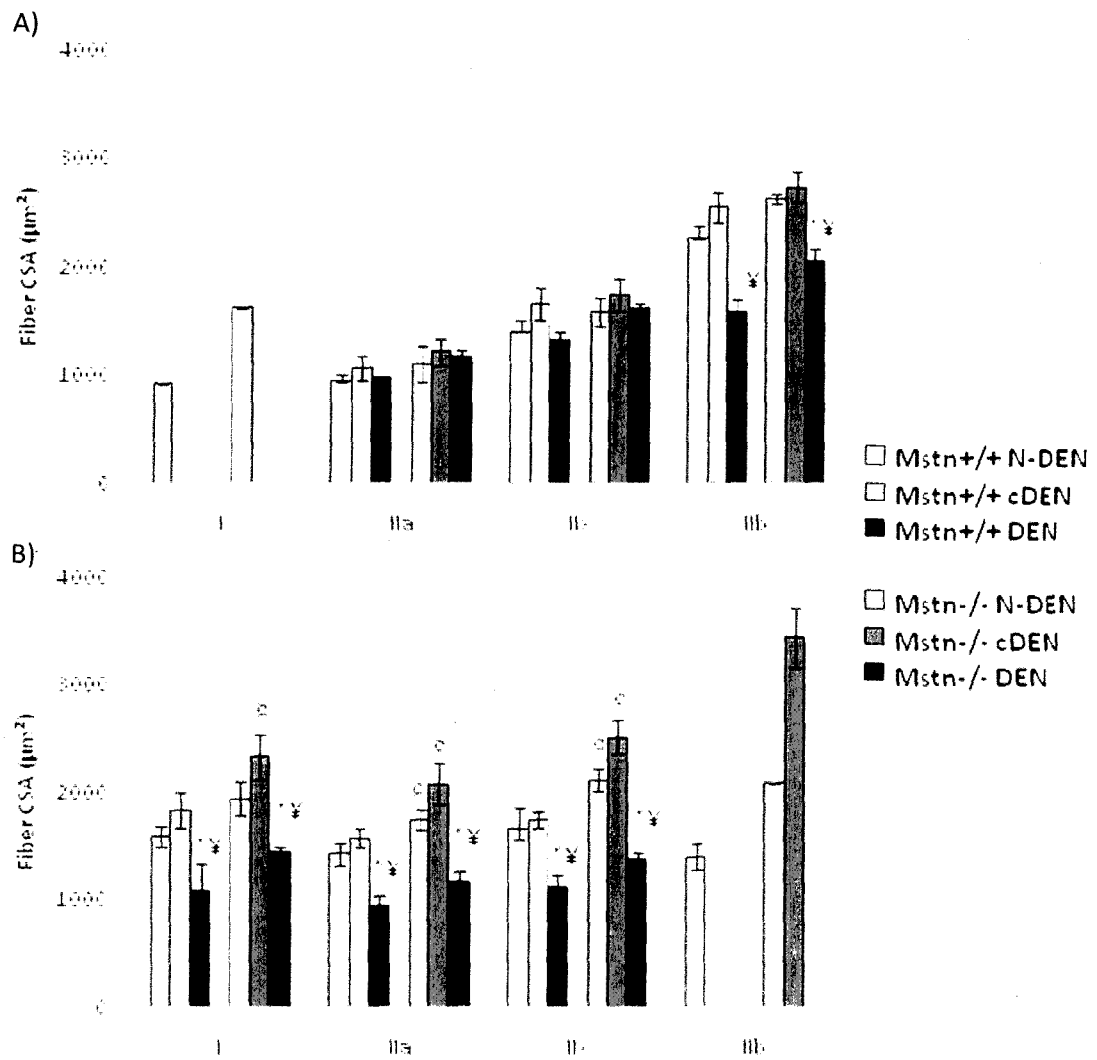


Figure 15 CSA of muscle fibers following 2 weeks of denervation

Fiber CSA in A) plantaris and B) soleus muscles. Values are means \pm S.E. n=3-4 per treatment group. α different from wildtype (*Mstn*^{+/+}) (p<0.05). * Different from non-denervated control (p<0.05). γ Different from contralateral limb (p<0.05).

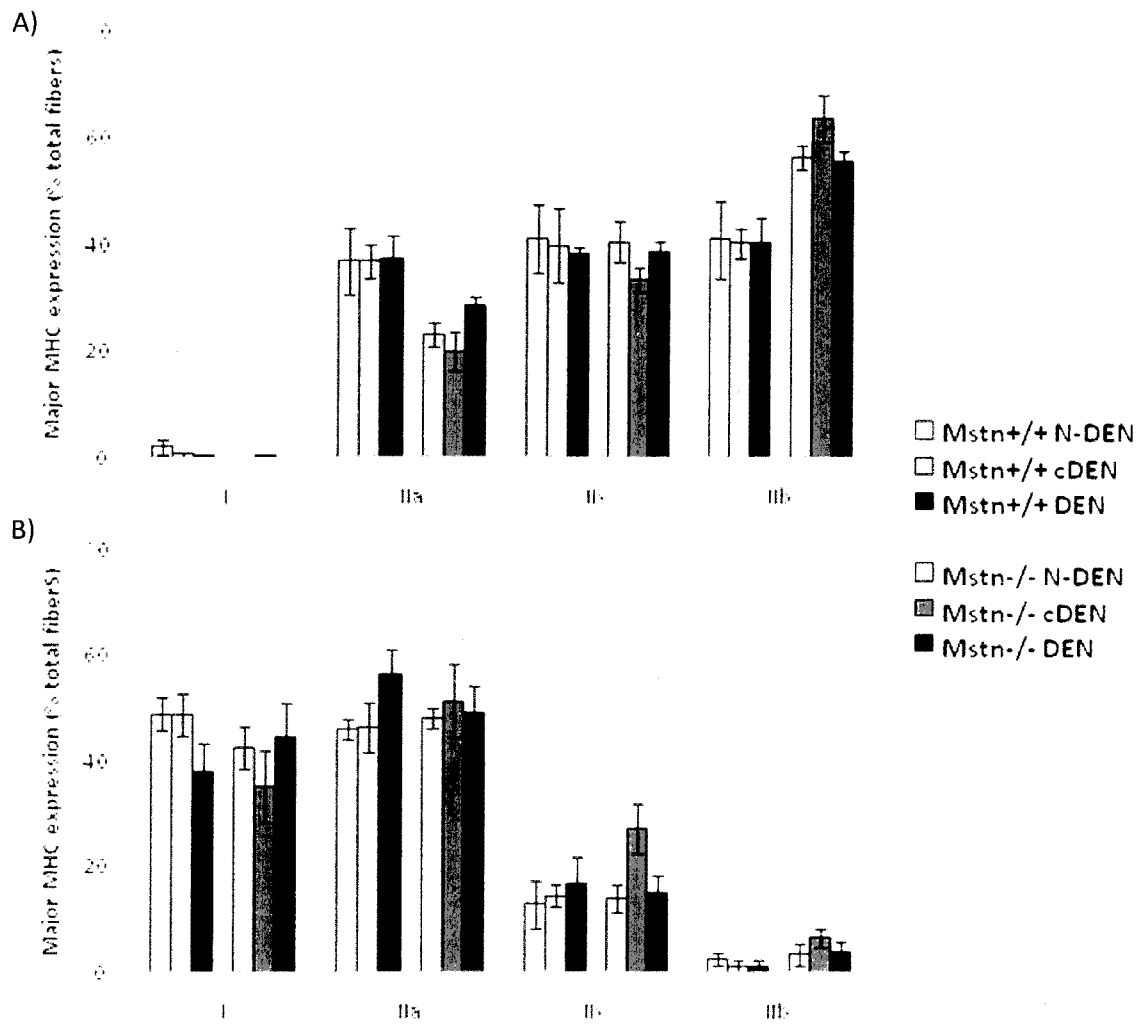


Figure 16 Expression of major MyHC isoforms after 2 weeks of denervation
 Major MyHC expression in A) plantaris and B) soleus muscles. Values are means \pm S.E. n=3-4 per treatment group.

Discussion

In the present study, we compared the atrophic response of plantaris and soleus muscle fibers in wildtype (*Mstn*^{+/+}) and *Mstn*^{-/-} mice. Treatments inhibiting the myostatin pathway have previously been successfully used in muscular dystrophy and sarcopenia[12, 13]. Myostatin also interacts with Akt and FoxO to modulate hypertrophy and atrophy. Therefore, we speculated that *Mstn*^{-/-} mice would not lose as much muscle mass as *Mstn*^{+/+} mice.

To date, the only studies looking at the rescuing effects of skeletal muscle atrophy have used the glucocorticoid or unloading model[187, 188]. When treated with glucocorticoids, the removal of myostatin was effective at preserving muscle mass [187]. Opposing this study, disuse atrophy was not prevented by myostatin deficiency [188]. In fact, more muscle mass was lost in mice lacking myostatin. Interestingly, hindlimb suspension did not cause any atrophy in the soleus muscle of *Mstn*^{+/+} mice[188]. We report that the absence of myostatin does not prevent atrophy induced by denervation. This was supported by the similar response in wildtype (*Mstn*^{+/+}) and *Mstn*^{-/-} mice of muscle mass loss and decrease in CSA of individual fibers.

Additionally, the proportions of the different isoforms of MyHCs did not change significantly after the experimental period in both plantaris and soleus muscles. Our findings match a recent study where changes in MyHC I were not observed following 1 month of denervation in mice[105]. The half-life of MyHCs is approximately two weeks[190] and, therefore, changes in the MyHC expression might not have been

detectable within our experimental design. The soleus muscle did, however, show a trend towards a faster phenotype.

The absence of myostatin in the soleus muscle could explain our results[81]. The plantaris does have myostatin, however, atrophy in *Mstn*^{-/-} mice was not spared either. Furthermore, myostatin mRNA was found to be upregulated after 1 day of hindlimb suspension but returned to basal levels on the 3rd day despite progressive atrophy of hindlimb muscles[81].

The secretion of myostatin into the bloodstream suggests that myostatin could potentially have a systemic role in signaling. Serum levels of myostatin have been assessed in heart dysfunction[191, 192]. The Western presented in this manuscript To date, no study has looked at serum levels of myostatin induced by atrophy in skeletal muscle. Therefore, it would be very important to assess changes of myostatin levels in both skeletal muscles and serum. Additionally, activin IIb receptor have been located on different organs including brain, adipose tissue, ovaries and testis[193, 194]. Whether myostatin signals through these receptors is still unknown, however, future studies could reveal novel roles of myostatin.

In light of these results, we suspect another signaling pathway might take precedence over the myostatin pathway, possibly the activin or IGF-I/Akt pathway.

To properly understand the mechanisms by which myostatin mediates atrophy, further experiments are needed. First, whether similar levels of atrogenes are induced by denervation, immunoblots against MuRF1 and MAFbx should be determined. The

induction of MAFbx and MuRF1 are mediated by FoxO proteins and therefore, antibodies for the FoxOs and their phosphorylated forms may provide evidence for their involvement.

Just as myostatin, activin is known to bind to activin receptor IIb and activate the same signaling cascade through Smad2 and Smad3[18]. Activin is involved in muscle growth and can partially replace myostatin's function in its absence[187]. Thus, whether activin or another ligand is activating the atrophy pathway through the Smad proteins needs to be determined.

Acknowledgements

I would like to thank Ewa Kulig, Stehpanie Michel and Mohammad Al-Khalaf for their technical support for the surgeries, extractions and analysis of tissues.

Chapter 4: Conclusion

In this thesis, I presented two preliminary manuscripts to elucidate myostatin's role on determining fiber size under conditions that either induce adult muscle growth or atrophy. In the absence of myostatin, muscle mass is greater. Knowledge about the regulatory processes involving myostatin is progressing, however, due to other pathways' involvement during growth a full understanding of these processes is lacking. In response to functional overload, we were expecting more muscle growth to occur in *Mstn*^{-/-} mice, but surprisingly, we found that the absence of myostatin leads to a different strategy being employed to achieve growth. We observed a blunted muscle growth in *Mstn*^{-/-} mice compared to wildtype counterparts. *Mstn*^{-/-} mice displayed more muscle damage in response to functional overload which resulted in a greater hyperplasia response through satellite cell activation and proliferation. On the other hand, we thought myostatin might save muscles from denervation-induced atrophy, but unfortunately muscles from *Mstn*^{-/-} mice were not spared with similar losses of muscle mass and cross-sectional area in both wildtype and *Mstn*^{-/-} mice. This suggests other regulatory processes are in place to compensate for the lack of myostatin. Further experiments are required to discover which pathway took precedence over myostatin. These findings have implications in nerve-mediated atrophy and paralysis in humans where myostatin treatment might not be beneficial. Further on, recent findings about myostatin therapy have raised interest in sports. Besides the doping issue, the potential muscle growth could improve sports performances. Unfortunately, the highly regenerative potential of satellite cells could

eventually be depleted after increased proliferation due to myostatin removal[13].

Although aged mice lacking myostatin display a greater number of satellite cells and their regenerative capacity is better than their age-matched wild type counterparts[13], little is known about long term effect on satellite cell population in humans.

In conclusion, this thesis shows that myostatin is not the only regulator of adult skeletal muscle mass in both growth and atrophy. Other pathways or regulatory protein must function in synergy or in parallel with myostatin to control muscle mass. This type of redundancy is very common in biology and serves to compensate for the absence or malfunction of a specific gene[195].

References

1. Crick, F., *Central Dogma of Molecular Biology*. Nature, 1970. **227**(5258): p. 561-563.
2. McPherron, A.C., A.M. Lawler, and S.J. Lee, *Regulation of skeletal muscle mass in mice by a new TGF- β superfamily member*. Nature, 1997. **387**(6628): p. 83-90.
3. Kambadur, R., M. Sharma, T.P.L. Smith, and J.J. Bass, *Mutations in myostatin (GDF8) in Double-Muscled Belgian Blue and Piedmontese Cattle*. Genome Research, 1997. **7**(9): p. 910-915.
4. Grobet, L., L.J. Royo Martin, D. Poncelet, D. Pirottin, B. Brouwers, J. Riquet, A. Schoeberlein, S. Dunner, F. Menissier, J. Massabanda, R. Fries, R. Hanset, and M. Georges, *A deletion in the bovine myostatin gene causes the double-muscled phenotype in cattle*. Nat Genet, 1997. **17**(1): p. 71-74.
5. Clop, A., F. Marcq, H. Takeda, D. Pirottin, X. Tordoir, B. Bibé, J. Bouix, F. Caiment, J.-M. Elsen, F. Eychenne, C. Larzul, E. Laville, F. Meish, D. Milenkovic, J. Tobin, C. Charlier, and M. Georges, *A mutation creating a potential illegitimate microRNA target site in the myostatin gene affects muscularity in sheep*. Nature Genetics, 2006. **38**(7): p. 813-818.
6. Schuelke, M., K.R. Wagner, L.E. Stolz, C. Hubner, T. Riebel, W. Komen, T. Braun, J.F. Tobin, and S.-J. Lee, *Myostatin Mutation Associated with Gross Muscle Hypertrophy in a Child*. N Engl J Med, 2004. **350**(26): p. 2682-2688.
7. McPherron, A.C. and S.-J. Lee, *Double muscling in cattle due to mutations in the myostatin gene*. Proceedings of the National Academy of Sciences of the United States of America, 1997. **94**(23): p. 12457-12461.
8. McPherron, A.C. and S.-J. Lee, *Suppression of body fat accumulation in myostatin-deficient mice*. The Journal of Clinical Investigation, 2002. **109**(5): p. 595-601.
9. Guo, T., W. Jou, T. Chanturiya, J. Portas, O. Gavrilova, and A.C. McPherron, *Myostatin Inhibition in Muscle, but Not Adipose Tissue, Decreases Fat Mass and Improves Insulin Sensitivity*. PLoS ONE, 2009. **4**(3): p. e4937.
10. Bogdanovich, S., T.O.B. Krag, E.R. Barton, L.D. Morris, L.-A. Whittemore, R.S. Ahima, and T.S. Khurana, *Functional improvement of dystrophic muscle by myostatin blockade*. Nature, 2002. **420**(6914): p. 418-421.
11. Kollias, H.D. and J.C. McDermott, *Transforming growth factor- β and myostatin signaling in skeletal muscle*. J Appl Physiol, 2008. **104**(3): p. 579-587.
12. Qiao, C., J. Li, J. Jiang, X. Zhu, B. Wang, J. Li, and X. Xiao, *Myostatin Propeptide Gene Delivery by Adeno-Associated Virus Serotype 8 Vectors Enhances Muscle Growth and Ameliorates Dystrophic Phenotypes in mdx Mice*. Human Gene Therapy, 2008. **19**(3): p. 241-254.
13. Siriett, V., L. Platt, M. Senna, S.N. Ling, R. Kambadur, and M. Sharma, *Prolonged absence of myostatin reduces sarcopenia*. Journal of Cellular Physiology, 2006. **209**(3): p. 866-873.
14. Hu, S., C. Chen, J. Sheng, Y. Sun, X. Cao, and J. Qiao, *Enhanced muscle growth by plasmid-mediated delivery of myostatin propeptide*. J Biomed Biotechnol, 2010: p. doi:10.1155/2010/862591.
15. Feng, X.-H. and R. Derynck, *Specificity and versatility in TGF- β signaling through Smags*. Annual Review of Cell and Developmental Biology, 2005. **21**(1): p. 659-693.

16. Tries, R.S., T. Chen, M.V. Da Vies, K.N. Tomkinson, A.A. Pearson, Q.A. Shakey, and N.M. Wolfman, *Gdf-8 Propeptide Binds to GDF-8 and Antagonizes Biological Activity by Inhibiting GDF-8 Receptor Binding*. Growth Factors, 2001. **18**(4): p. 251 - 259.
17. Hill, J.J., M.V. Davies, A.A. Pearson, J.H. Wang, R.M. Hewick, N.M. Wolfman, and Y. Qiu, *The Myostatin Propeptide and the Follistatin-related Gene Are Inhibitory Binding Proteins of Myostatin in Normal Serum*. J. Biol. Chem., 2002. **277**(43): p. 40735-40741.
18. Dijke, P.T., M.-J. Goumans, F. Itoh, and S. Itoh, *Regulation of cell proliferation by Smad proteins*. Journal of Cellular Physiology, 2002. **191**(1): p. 1-16.
19. Massagué, J., *TGF- β Signal transduction*. Annual Review of Biochemistry, 1998. **67**(1): p. 753-791.
20. Rebbapragada, A., H. Benchabane, J.L. Wrana, A.J. Celeste, and L. Attisano, *Myostatin Signals through a Transforming Growth Factor β -Like Signaling Pathway To Block Adipogenesis*. Mol. Cell. Biol., 2003. **23**(20): p. 7230-7242.
21. Forbes, D., M. Jackman, A. Bishop, M. Thomas, R. Kambadur, and M. Sharma, *Myostatin auto-regulates its expression by feedback loop through Smad7 dependent mechanism*. Journal of Cellular Physiology, 2006. **206**(1): p. 264-272.
22. Buckingham, M., *Muscle Differentiation: Which myogenic factors make muscle?* Current Biology, 1994. **4**(1): p. 61-63.
23. Pownall, M.E., M.K. Gustafsson, and C.P. Emerson, *Myogenic regulatory factors and the specification of muscle progenitors in vertebrate embryos*. Annual Review of Cell & Developmental Biology, 2002. **18**(1): p. 747.
24. Rudnicki, M.A., F. Le Grand, I. McKinnell, and S. Kuang, *The Molecular Regulation of Muscle Stem Cell Function*. Cold Spring Harbor Symposia on Quantitative Biology, 2008. **73**: p. 323-331.
25. Sabourin, L.A. and M.A. Rudnicki, *The molecular regulation of myogenesis*. Clinical Genetics, 2000. **57**(1): p. 16-25.
26. Ishibashi, J., R.L. Perry, A. Asakura, and M.A. Rudnicki, *MyoD induces myogenic differentiation through cooperation of its NH₂- and COOH-terminal regions*. J. Cell Biol., 2005. **171**(3): p. 471-482.
27. Cao, Y., R.M. Kumar, B.H. Penn, C.A. Berkes, C. Kooperberg, L.A. Boyer, R.A. Young, and S.J. Tapscott, *Global and gene-specific analyses show distinct roles for Myod and Myog at a common set of promoters*. EMBO J, 2006. **25**(3): p. 502-511.
28. Zhang, W., R.R. Behringer, and E.N. Olson, *Inactivation of the myogenic bHLH gene MRF4 results in up-regulation of myogenin and rib anomalies*. Genes & Development, 1995. **9**(11): p. 1388-1399.
29. Ferri, P., E. Barbieri, S. Burattini, M. Guescini, A. D'Emilio, L. Biagiotti, P. Del Grande, A. De Luca, V. Stocchi, and E. Falcieri, *Expression and subcellular localization of myogenic regulatory factors during the differentiation of skeletal muscle C2C12 myoblasts*. Journal of Cellular Biochemistry, 2009. **108**(6): p. 1302-1317.
30. Bischoff, R., *The satellite cell and muscle regeneration*, in *Myogenesis*, A.G. Engel and C. Franzini-Armstrong, Editors. 1994, McGraw-Hill: New York. p. 97-118.
31. Tidball, J.G. and M. Wehling-Henricks, *Macrophages promote muscle membrane repair and muscle fibre growth and regeneration during modified muscle loading in mice in vivo*. The Journal of Physiology, 2007. **578**(1): p. 327-336.
32. Salleo, A., G. Anastasi, G.L. Spada, G. Falzea, and M.G. Denaro, *New muscle fiber production during compensatory hypertrophy*. Medicine & Science in Sports & Exercise, 1980. **12**(4): p. 268-273.

33. Tamaki, T., A. Akatsuka, M. Tokunaga, K. Ishige, S. Uchiyama, and T. Shiraishi, *Morphological and biochemical evidence of muscle hyperplasia following weight-lifting exercise in rats*. *Am J Physiol Cell Physiol*, 1997. **273**(1): p. C246-256.
34. Hill, M., A. Wernig, and G. Goldspink, *Muscle satellite (stem) cell activation during local tissue injury and repair*. *Journal of Anatomy*, 2003. **203**(1): p. 89-99.
35. Schultz, E., D.L. Jaryszak, M.C. Gibson, and D.J. Albright, *Absence of exogenous satellite cell contribution to regeneration of frozen skeletal muscle*. *Journal of Muscle Research and Cell Motility*, 1986. **7**(4): p. 361-367.
36. Oustanina, S., G. Hause, and T. Braun, *Pax7 directs postnatal renewal and propagation of myogenic satellite cells but not their specification*. *EMBO J*, 2004. **23**(16): p. 3430-3439.
37. Relaix, F., D. Montarras, S. Zaffran, B. Gayraud-Morel, D. Rocancourt, S. Tajbakhsh, A. Mansouri, A. Cumano, and M. Buckingham, *Pax3 and Pax7 have distinct and overlapping functions in adult muscle progenitor cells*. *J. Cell Biol.*, 2006. **172**(1): p. 91-102.
38. Lagha, M., T. Sato, L. Bajard, P. Daubas, M. Esner, D. Montarras, F. Relaix, and M. Buckingham, *Regulation of Skeletal Muscle Stem Cell Behavior by Pax3 and Pax7*. *Cold Spring Harbor Symposia on Quantitative Biology*, 2008. **73**: p. 307-315.
39. Buckingham, M. and F.d.r. Relaix, *The Role of Pax Genes in the Development of Tissues and Organs: Pax3 and Pax7 Regulate Muscle Progenitor Cell Functions*. *Annual Review of Cell and Developmental Biology*, 2007. **23**(1): p. 645-673.
40. Schultz, E., *A quantitative study of the satellite cell population in postnatal mouse lumbrical muscle*. *Anat Rec*, 1974. **180**(4): p. 589-95.
41. Hellmuth, A.E. and D.B. Allbrook, *Muscle satellite cell numbers during the postnatal period*. *J Anat*, 1971. **110**(Pt 3): p. 503.
42. Allbrook, D.B., M.F. Han, and A.E. Hellmuth, *Population of muscle satellite cells in relation to age and mitotic activity*. *Pathology*, 1971. **3**(3): p. 223-43.
43. Scime, A., A.Z. Caron, and G. Grenier, *Advances in myogenic cell transplantation and skeletal muscle tissue engineering*. *Front Biosci*, 2009. **14**: p. 3012-23.
44. Zammit, P.S., T.A. Partridge, and Z. Yablonka-Reuveni, *The Skeletal Muscle Satellite Cell: The Stem Cell That Came in From the Cold*. *J. Histochem. Cytochem.*, 2006. **54**(11): p. 1177-1191.
45. Thomas, M., B. Langley, C. Berry, M. Sharma, S. Kirk, J. Bass, and R. Kambadur, *Myostatin, a Negative Regulator of Muscle Growth, Functions by Inhibiting Myoblast Proliferation*. *Journal of Biological Chemistry*, 2000. **275**(51): p. 40235-40243.
46. Rios, R., I. Carneiro, V.M. Arce, and J. Devesa, *Myostatin is an inhibitor of myogenic differentiation*. *Am J Physiol Cell Physiol*, 2002. **282**(5): p. C993-999.
47. Langley, B., M. Thomas, A. Bishop, M. Sharma, S. Gilmour, and R. Kambadur, *Myostatin Inhibits Myoblast Differentiation by Down-regulating MyoD Expression*. *Journal of Biological Chemistry*, 2002. **277**(51): p. 49831-49840.
48. Liu, D., B.L. Black, and R. Derynck, *TGF- β inhibits muscle differentiation through functional repression of myogenic transcription factors by Smad3*. *Genes & Development*, 2001. **15**(22): p. 2950-2966.
49. McCroskery, S., M. Thomas, L. Maxwell, M. Sharma, and R. Kambadur, *Myostatin negatively regulates satellite cell activation and self-renewal*. *J. Cell Biol.*, 2003. **162**(6): p. 1135-1147.
50. McFarlane, C., A. Hennebry, M. Thomas, E. Plummer, N. Ling, M. Sharma, and R. Kambadur, *Myostatin signals through Pax7 to regulate satellite cell self-renewal*. *Experimental Cell Research*, 2008. **314**(2): p. 317-329.

51. Amthor, H., A. Otto, A. Vulin, A. Rochat, J. Dumonceaux, L. Garcia, E. Mouisel, C. Hourdé, R. Macharia, M. Friedrichs, F. Relaix, P.S. Zammit, A. Matsakas, K. Patel, and T. Partridge, *Muscle hypertrophy driven by myostatin blockade does not require stem/precursor-cell activity*. Proceedings of the National Academy of Sciences, 2009. **106**(18): p. 7479-7484.
52. Turner, J.D., P. Rotwein, J. Novakofski, and P.J. Bechtel, *Induction of mRNA for IGF-I and -II during growth hormone-stimulated muscle hypertrophy*. Am J Physiol Endocrinol Metab, 1988. **255**(4): p. E513-517.
53. Murgia, M., A.L. Serrano, E. Calabria, G. Pallafacchina, T. Lomo, and S. Schiaffino, *Ras is involved in nerve-activity-dependent regulation of muscle genes*. Nat Cell Biol, 2000. **2**(3): p. 142-147.
54. Bodine, S.C., T.N. Stitt, M. Gonzalez, W.O. Kline, G.L. Stover, R. Bauerlein, E. Zlotchenko, A. Scrimgeour, J.C. Lawrence, D.J. Glass, and G.D. Yancopoulos, *Akt/mTOR pathway is a crucial regulator of skeletal muscle hypertrophy and can prevent muscle atrophy in vivo*. Nat Cell Biol, 2001. **3**(11): p. 1014-1019.
55. Spangenburg, E.E., D. Le Roith, C.W. Ward, and S.C. Bodine, *A functional insulin-like growth factor receptor is not necessary for load-induced skeletal muscle hypertrophy*. The Journal of Physiology, 2008. **586**(1): p. 283-291.
56. Adams, G.R., *Exercise Effects on Muscle Insulin Signaling and Action: Invited Review: Autocrine/paracrine IGF-I and skeletal muscle adaptation*. J Appl Physiol, 2002. **93**(3): p. 1159-1167.
57. Barton-Davis, E.R., D.I. Shoturma, and H.L. Sweeney, *Contribution of satellite cells to IGF-I induced hypertrophy of skeletal muscle*. Acta Physiologica Scandinavica, 1999. **167**(4): p. 301-305.
58. Rosenblatt, J.D., D. Yong, and D.J. Parry, *Satellite cell activity is required for hypertrophy of overloaded adult rat muscle*. Muscle & Nerve, 1994. **17**(6): p. 608-613.
59. Phelan, J.N. and W.J. Gonyea, *Effect of radiation on satellite cell activity and protein expression in overloaded mammalian skeletal muscle*. The Anatomical Record, 1997. **247**(2): p. 179-188.
60. Blaauw, B., M. Canato, L. Agatea, L. Toniolo, C. Mammucari, E. Masiero, R. Abraham, M. Sandri, S. Schiaffino, and C. Reggiani, *Inducible activation of Akt increases skeletal muscle mass and force without satellite cell activation*. FASEB J., 2009: p. fj.09-131870.
61. Morissette, M., S. Cook, C. Buranasombati, M. Rosenberg, and A. Rosenzweig, *Myostatin Inhibits IGF-I Induced Myotube Hypertrophy Through Akt*. Am J Physiol Cell Physiol, 2009: p. ajpcell.00043.2009.
62. Trendelenburg, A.U., A. Meyer, D. Rohner, J. Boyle, S. Hatakeyama, and D.J. Glass, *Myostatin reduces Akt/TORC1/p70S6K signaling, inhibiting myoblast differentiation and myotube size*. Am J Physiol Cell Physiol, 2009. **296**(6): p. C1258-1270.
63. Otto, A. and K. Patel, *Signalling and the control of skeletal muscle size*. Experimental Cell Research, 2010. **In Press, Corrected Proof**.
64. Sandri, M., *Signaling in Muscle Atrophy and Hypertrophy*. Physiology, 2008. **23**(3): p. 160-170.
65. McCarthy, J.J. and K.A. Esser, *Anabolic and catabolic pathways regulating skeletal muscle mass*. Current Opinion in Clinical Nutrition & Metabolic Care, 2010. **13**(3): p. 230-235 10.1097/MCO.0b013e32833781b5.
66. Satchek, J.M., J.-P.K. Hyatt, A. Raffaello, R.T. Jagoe, R.R. Roy, V.R. Edgerton, S.H. Lecker, and A.L. Goldberg, *Rapid disuse and denervation atrophy involve transcriptional changes similar to those of muscle wasting during systemic diseases*. FASEB J., 2007. **21**(1): p. 140-155.

67. Bodine, S.C., E. Latres, S. Baumhueter, V.K.M. Lai, L. Nunez, B.A. Clarke, W.T. Poueymirou, F.J. Panaro, E. Na, K. Dharmarajan, Z.-Q. Pan, D.M. Valenzuela, T.M. DeChiara, T.N. Stitt, G.D. Yancopoulos, and D.J. Glass, *Identification of Ubiquitin Ligases Required for Skeletal Muscle Atrophy*. *Science*, 2001. **294**(5547): p. 1704-1708.
68. Gomes, M.D., S.H. Lecker, R.T. Jagoe, A. Navon, and A.L. Goldberg, *Atrogin-1, a muscle-specific F-box protein highly expressed during muscle atrophy*. *Proceedings of the National Academy of Sciences of the United States of America*, 2001. **98**(25): p. 14440-14445.
69. Ciechanover, A., *The ubiquitin-proteasome pathway: on protein death and cell life*. *EMBO J*, 1998. **17**(24): p. 7151-7160.
70. Tawa, N.E., R. Odessey, and A.L. Goldberg, *Inhibitors of the proteasome reduce the accelerated proteolysis in atrophying rat skeletal muscles*. *The Journal of Clinical Investigation*, 1997. **100**(1): p. 197-203.
71. Lagirand-Cantaloube, J., K. Cornille, A. Csibi, S. Batonnet-Pichon, M.P. Leibovitch, and S.A. Leibovitch, *Inhibition of Atrogin-1/MAFbx Mediated MyoD Proteolysis Prevents Skeletal Muscle Atrophy In Vivo*. *PLoS ONE*, 2009. **4**(3): p. e4973.
72. Jogo, M., S. Shiraishi, and T.-a. Tamura, *Identification of MAFbx as a myogenin-engaged F-box protein in SCF ubiquitin ligase*. *FEBS Letters*, 2009. **583**(17): p. 2715-2719.
73. Cohen, S., J.J. Brault, S.P. Gygi, D.J. Glass, D.M. Valenzuela, C. Gartner, E. Latres, and A.L. Goldberg, *During muscle atrophy, thick, but not thin, filament components are degraded by MuRF1-dependent ubiquitylation*. *J. Cell Biol.*, 2009. **185**(6): p. 1083-1095.
74. Sandri, M., C. Sandri, A. Gilbert, C. Skurk, E. Calabria, A. Picard, K. Walsh, S. Schiaffino, S.H. Lecker, and A.L. Goldberg, *Foxo Transcription Factors Induce the Atrophy-Related Ubiquitin Ligase Atrogin-1 and Cause Skeletal Muscle Atrophy*. *Cell*, 2004. **117**(3): p. 399-412.
75. Stitt, T.N., D. Drujan, B.A. Clarke, F. Panaro, Y. Timofeyva, W.O. Kline, M. Gonzalez, G.D. Yancopoulos, and D.J. Glass, *The IGF-1/PI3K/Akt Pathway Prevents Expression of Muscle Atrophy-Induced Ubiquitin Ligases by Inhibiting FOXO Transcription Factors*. *Molecular Cell*, 2004. **14**(3): p. 395-403.
76. Glass, D.J., *Skeletal muscle hypertrophy and atrophy signaling pathways*. *The International Journal of Biochemistry & Cell Biology*, 2005. **37**(10): p. 1974-1984.
77. Kamei, Y., S. Miura, M. Suzuki, Y. Kai, J. Mizukami, T. Taniguchi, K. Mochida, T. Hata, J. Matsuda, H. Aburatani, I. Nishino, and O. Ezaki, *Skeletal Muscle FOXO1 (FKHR) Transgenic Mice Have Less Skeletal Muscle Mass, Down-regulated Type I (Slow Twitch/Red Muscle) Fiber Genes, and Impaired Glycemic Control*. *Journal of Biological Chemistry*, 2004. **279**(39): p. 41114-41123.
78. Baumann, A.P., C. Ibebunjo, W.A. Grasser, and V.M. Paralkar, *Myostatin expression in age and denervation-induced skeletal muscle atrophy*. *J Musculoskelet Neuronal Interact*, 2003. **3**(1): p. 8-16.
79. Shao, C., M. Liu, X. Wu, and F. Ding, *Time-dependent expression of myostatin RNA transcript and protein in gastrocnemius muscle of mice after sciatic nerve resection*. *Microsurgery*, 2007. **27**(5): p. 487-493.
80. Gonzalez-Cadavid, N.F., W.E. Taylor, K. Yarasheski, I. Sinha-Hikim, K. Ma, S. Ezzat, R. Shen, R. Lalani, S. Asa, M. Mamita, G. Nair, S. Arver, and S. Bhasin, *Organization of the human myostatin gene and expression in healthy men and HIV-infected men with muscle wasting*. *Proceedings of the National Academy of Sciences of the United States of America*, 1998. **95**(25): p. 14938-14943.

81. Carlson, C.J., F.W. Booth, and S.E. Gordon, *Skeletal muscle myostatin mRNA expression is fiber-type specific and increases during hindlimb unloading*. *Am J Physiol Regul Integr Comp Physiol*, 1999. **277**(2): p. R601-606.
82. Allen, D.L. and T.G. Unterman, *Regulation of myostatin expression and myoblast differentiation by FoxO and SMAD transcription factors*. *Am J Physiol Cell Physiol*, 2007. **292**(1): p. C188-199.
83. McFarlane, C., E. Plummer, M. Thomas, A. Hennebry, M. Ashby, N. Ling, H. Smith, M. Sharma, and R. Kambadur, *Myostatin induces cachexia by activating the ubiquitin proteolytic system through an NF-kappaB-independent, FoxO1-dependent mechanism*. *Journal of Cellular Physiology*, 2006. **209**(2): p. 501-514.
84. Salerno, M.S., M. Thomas, D. Forbes, T. Watson, R. Kambadur, and M. Sharma, *Molecular analysis of fiber type-specific expression of murine myostatin promoter*. *Am J Physiol Cell Physiol*, 2004. **287**(4): p. C1031-1040.
85. Girgenrath, S., K. Song, and L.-A. Whittemore, *Loss of myostatin expression alters fiber-type distribution and expression of myosin heavy chain isoforms in slow- and fast-type skeletal muscle*. *Muscle & Nerve*, 2005. **31**(1): p. 34-40.
86. Hennebry, A., C. Berry, V. Siriatt, P. O'Callaghan, L. Chau, T. Watson, M. Sharma, and R. Kambadur, *Myostatin regulates fiber-type composition of skeletal muscle by regulating MEF2 and MyoD gene expression*. *Am J Physiol Cell Physiol*, 2009. **296**(3): p. C525-534.
87. Hyatt, J.-P.K., G.E. McCall, E.M. Kander, H. Zhong, R.R. Roy, and K.A. Huey, *PAX3/7 expression coincides with myod during chronic skeletal muscle overload*. *Muscle & Nerve*, 2008. **38**(1): p. 861-866.
88. Baldwin, K.M., V. Valdez, L.F. Schrader, and R.E. Herrick, *Effect of functional overload on substrate oxidation capacity of skeletal muscle*. *J Appl Physiol*, 1981. **50**(6): p. 1272-1276.
89. Dunn, S.E. and R.N. Michel, *Coordinated expression of myosin heavy chain isoforms and metabolic enzymes within overloaded rat muscle fibers*. *Am J Physiol Cell Physiol*, 1997. **273**(2): p. C371-383.
90. Dunn, S.E., E.R. Chin, and R.N. Michel, *Matching of Calcineurin Activity to Upstream Effectors Is Critical for Skeletal Muscle Fiber Growth*. *J. Cell Biol.*, 2000. **151**(3): p. 663-672.
91. Dunn, S.E., J.L. Burns, and R.N. Michel, *Calcineurin Is Required for Skeletal Muscle Hypertrophy*. *J. Biol. Chem.*, 1999. **274**(31): p. 21908-21912.
92. Armstrong, R.B., P. Marum, P. Tullson, and C.W.t. Saubert, *Acute hypertrophic response of skeletal muscle to removal of synergists*. *J Appl Physiol*, 1979. **46**(4): p. 835-842.
93. Tidball, J.G., E. Berchenko, and J. Frenette, *Macrophage invasion does not contribute to muscle membrane injury during inflammation*. *J Leukoc Biol*, 1999. **65**(4): p. 492-498.
94. Adams, G.R., F. Haddad, and K.M. Baldwin, *Time course of changes in markers of myogenesis in overloaded rat skeletal muscles*. *J Appl Physiol*, 1999. **87**(5): p. 1705-1712.
95. Rommel, C., S.C. Bodine, B.A. Clarke, R. Rossman, L. Nunez, T.N. Stitt, G.D. Yancopoulos, and D.J. Glass, *Mediation of IGF-1-induced skeletal myotube hypertrophy by PI(3)K/Akt/mTOR and PI(3)K/Akt/GSK3 pathways*. *Nat Cell Biol*, 2001. **3**(11): p. 1009-1013.
96. Musaro, A., K. McCullagh, A. Paul, L. Houghton, G. Dobrowolny, M. Molinaro, E.R. Barton, H. L Sweeney, and N. Rosenthal, *Localized Igf-1 transgene expression sustains hypertrophy and regeneration in senescent skeletal muscle*. *Nat Genet*, 2001. **27**(2): p. 195-200.

97. Yamaguchi, A., Y. Ikeda, T. Hirai, T. Fujikawa, and I. Morita, *Local changes of IGF-I mRNA, GH receptor mRNA, and fiber size in rat plantaris muscle following compensatory overload*. *Jpn J Physiol*, 2003. **53**(1): p. 53-60.
98. Yamaguchi, A., T. Fujikawa, S. Shimada, I. Kanbayashi, M. Tateoka, H. Soya, H. Takeda, I. Morita, K. Matsubara, and T. Hirai, *Muscle IGF-I E α , MGF, and myostatin mRNA expressions after compensatory overload in hypophysectomized rats*. *Pflügers Archiv European Journal of Physiology*, 2006. **453**(2): p. 203-210.
99. McCall, G.E., D.L. Allen, J.K. Linderman, R.E. Grindeland, R.R. Roy, V.R. Mukku, and V.R. Edgerton, *Maintenance of myonuclear domain size in rat soleus after overload and growth hormone/IGF-I treatment*. *J Appl Physiol*, 1998. **84**(4): p. 1407-1412.
100. Schiaffino, S., S. Pierobon Bormioli, and M. Aloisi, *The fate of newly formed satellite cells during compensatory muscle hypertrophy*. *Virchows Archiv B Cell Pathology Zell-pathologie*, 1976. **21**(1): p. 113-118.
101. Bigard, A.X., J. Zoll, F. Ribera, P. Mateo, H. Sanchez, B. Serrurier, and R. Ventura-Clapier, *Influence of overload on phenotypic remodeling in regenerated skeletal muscle*. *Am J Physiol Cell Physiol*, 2001. **281**(5): p. C1686-1694.
102. Savage, K.J. and A.C. McPherron, *Endurance exercise training in myostatin null mice*. *Muscle & Nerve*, 2010: p. n/a-n/a.
103. Matsakas, A., E. Mouisel, H. Amthor, and K. Patel, *Myostatin knockout mice increase oxidative muscle phenotype as an adaptive response to exercise*. *Journal of Muscle Research and Cell Motility*, 2010. **31**(2): p. 111-125.
104. Personius, K.E., A. Jayaram, D. Krull, R. Brown, T. Xu, B. Han, K. Burgess, C. Storey, B. Shah, R. Tawil, and S. Welle, *Grip force, EDL contractile properties, and voluntary wheel running after postdevelopmental myostatin depletion in mice*. *J Appl Physiol*, 2010: p. japplphysiol.00300.2010.
105. Agbulut, O., A. Vignaud, C. Hourde, E. Mouisel, F. Fougereuse, G.S. Butler-Browne, and A. Ferry, *Slow myosin heavy chain expression in the absence of muscle activity*. *Am J Physiol Cell Physiol*, 2009. **296**(1): p. C205-214.
106. Michel, R.N., D.J. Parry, and S.E. Dunn, *Regulation of myosin heavy chain expression in adult rat hindlimb muscles during short-term paralysis: comparison of denervation and tetrodotoxin-induced neural inactivation*. *FEBS Letters*, 1996. **391**(1-2): p. 39-44.
107. Huey, K.A. and S.C. Bodine, *Changes in myosin mRNA and protein expression in denervated rat soleus and tibialis anterior*. *European Journal of Biochemistry*, 1998. **256**(1): p. 45-50.
108. Huey, K.A., F. Haddad, A.X. Qin, and K.M. Baldwin, *Transcriptional regulation of the type I myosin heavy chain gene in denervated rat soleus*. *Am J Physiol Cell Physiol*, 2003. **284**(3): p. C738-748.
109. Sandri, M., J. Lin, C. Handschin, W. Yang, Z.P. Arany, S.H. Lecker, A.L. Goldberg, and B.M. Spiegelman, *PGC-1 α protects skeletal muscle from atrophy by suppressing FoxO3 action and atrophy-specific gene transcription*. *Proceedings of the National Academy of Sciences*, 2006. **103**(44): p. 16260-16265.
110. Zeman, R.J., J. Zhao, Y. Zhang, W. Zhao, X. Wen, Y. Wu, J. Pan, W.A. Bauman, and C. Cardozo, *Differential skeletal muscle gene expression after upper or lower motor neuron transection*. *Pflugers Arch*, 2009.
111. Waddell, D.S., L.M. Baehr, J. van den Brandt, S.A. Johnsen, H.M. Reichardt, J.D. Furlow, and S.C. Bodine, *The glucocorticoid receptor and FOXO1 synergistically activate the skeletal muscle atrophy-associated MuRF1 gene*. *Am J Physiol Endocrinol Metab*, 2008. **295**(4): p. E785-797.

112. Siu, P.M. and S.E. Alway, *Response and adaptation of skeletal muscle to denervation stress: the role of apoptosis in muscle loss*. Front Biosci, 2009. **14**: p. 432-52.
113. Borisov, A.B. and B.M. Carlson, *Cell death in denervated skeletal muscle is distinct from classical apoptosis*. The Anatomical Record, 2000. **258**(3): p. 305-318.
114. Midrio, M., *The denervated muscle: facts and hypotheses. A historical review*. European Journal of Applied Physiology, 2006. **98**(1): p. 1-21.
115. Midrio, M., D.D. Betto, R. Betto, D. Noventa, and F. Antico, *Cordotomy-denervation interactions on contractile and myofibrillar properties of fast and slow muscles in the rat*. Experimental Neurology, 1988. **100**(1): p. 216-236.
116. Lima, S.C.M.S., Q.M.M.S. Caierao, S.M.M.S. Peviani, T.L.M.S. Russo, M.C.M.S.P. Somazz, T.F.M.S.P. Salvini, R.M.M.S.P. Teodori, and V.B.M.S.P. Minamoto, *Muscle and Nerve Responses After Different Intervals of Electrical Stimulation Sessions on Denervated Rat Muscle*. American Journal of Physical Medicine & Rehabilitation, 2009. **88**(2): p. 126-135.
117. Czerwinski, S.M., J.A.N. Novakofski, and P.J. Bechtel, *Modulation of IGF mRNA abundance during muscle denervation atrophy*. Medicine & Science in Sports & Exercise, 1993. **25**(9): p. 1005-1008.
118. Lalani, R., S. Bhasin, F. Byhower, R. Tarnuzzer, M. Grant, R. Shen, S. Asa, S. Ezzat, and N.F. Gonzalez-Cadavid, *Myostatin and insulin-like growth factor-I and -II expression in the muscle of rats exposed to the microgravity environment of the NeuroLab space shuttle flight*. J Endocrinol, 2000. **167**(3): p. 417-428.
119. Allen, D.L., E.R. Bandstra, B.C. Harrison, S. Thorng, L.S. Stodieck, P.J. Kostenuik, S. Morony, D.L. Lacey, T.G. Hammond, L.L. Leinwand, W.S. Argraves, T.A. Bateman, and J.L. Barth, *Effects of spaceflight on murine skeletal muscle gene expression*. J Appl Physiol, 2009. **106**(2): p. 582-595.
120. Ma, K., C. Mallidis, S. Bhasin, V. Mahabadi, J. Artaza, N. Gonzalez-Cadavid, J. Arias, and B. Salehian, *Glucocorticoid-induced skeletal muscle atrophy is associated with upregulation of myostatin gene expression*. Am J Physiol Endocrinol Metab, 2003. **285**(2): p. E363-371.
121. Kambadur, R., M. Sharma, T.P. Smith, and J.J. Bass, *Mutations in myostatin (GDF8) in double-muscling Belgian Blue and Piedmontese cattle*. Genome Res, 1997. **7**(9): p. 910-6.
122. McPherron, A.C., A.M. Lawler, and S.J. Lee, *Regulation of skeletal muscle mass in mice by a new TGF-beta superfamily member*. Nature, 1997. **387**(6628): p. 83-90.
123. Lee, S.J., L.A. Reed, M.V. Davies, S. Girgenrath, M.E. Goad, K.N. Tomkinson, J.F. Wright, C. Barker, G. Ehrmantraut, J. Holmstrom, B. Trowell, B. Gertz, M.S. Jiang, S.M. Sebald, M. Matzuk, E. Li, L.F. Liang, E. Quattlebaum, R.L. Stotish, and N.M. Wolfman, *Regulation of muscle growth by multiple ligands signaling through activin type II receptors*. Proc Natl Acad Sci U S A, 2005. **102**(50): p. 18117-22.
124. Joulia, D., H. Bernardi, V. Garandel, F. Rabenoelina, B. Vernus, and G. Cabello, *Mechanisms involved in the inhibition of myoblast proliferation and differentiation by myostatin*. Exp Cell Res, 2003. **286**(2): p. 263-75.
125. Langley, B., M. Thomas, A. Bishop, M. Sharma, S. Gilmour, and R. Kambadur, *Myostatin inhibits myoblast differentiation by down-regulating MyoD expression*. J Biol Chem, 2002. **277**(51): p. 49831-40.
126. Rebbapragada, A., H. Benchabane, J.L. Wrana, A.J. Celeste, and L. Attisano, *Myostatin signals through a transforming growth factor beta-like signaling pathway to block adipogenesis*. Mol Cell Biol, 2003. **23**(20): p. 7230-42.

127. Zhu, X., S. Topouzis, L.F. Liang, and R.L. Stotish, *Myostatin signaling through Smad2, Smad3 and Smad4 is regulated by the inhibitory Smad7 by a negative feedback mechanism*. *Cytokine*, 2004. **26**(6): p. 262-72.
128. Amirouche, A., A.C. Durieux, S. Banzet, N. Koulmann, R. Bonnefoy, C. Mouret, X. Bigard, A. Peinnequin, and D. Freyssenet, *Down-regulation of Akt/mammalian target of rapamycin signaling pathway in response to myostatin overexpression in skeletal muscle*. *Endocrinology*, 2009. **150**(1): p. 286-94.
129. McFarlane, C., E. Plummer, M. Thomas, A. Hennebry, M. Ashby, N. Ling, H. Smith, M. Sharma, and R. Kambadur, *Myostatin induces cachexia by activating the ubiquitin proteolytic system through an NF-kappaB-independent, FoxO1-dependent mechanism*. *J Cell Physiol*, 2006. **209**(2): p. 501-14.
130. Morissette, M.R., S.A. Cook, C. Buranasombati, M.A. Rosenberg, and A. Rosenzweig, *Myostatin inhibits IGF-I-induced myotube hypertrophy through Akt*. *Am J Physiol Cell Physiol*, 2009. **297**(5): p. C1124-32.
131. Trendelenburg, A.U., A. Meyer, D. Rohner, J. Boyle, S. Hatakeyama, and D.J. Glass, *Myostatin reduces Akt/TORC1/p70S6K signaling, inhibiting myoblast differentiation and myotube size*. *Am J Physiol Cell Physiol*, 2009. **296**(6): p. C1258-70.
132. Baldwin, K.M., W.G. Cheadle, O.M. Martinez, and D.A. Cooke, *Effect of functional overload on enzyme levels in different types of skeletal muscle*. *J Appl Physiol*, 1977. **42**(2): p. 312-317.
133. Baldwin, K.M., W.G. Cheadle, O.M. Martinez, and D.A. Cooke, *Effect of functional overload on enzyme levels in different types of skeletal muscle*. *J Appl Physiol*, 1977. **42**(2): p. 312-7.
134. Baldwin, K.M., V. Valdez, L.F. Schrader, and R.E. Herrick, *Effect of functional overload on substrate oxidation capacity of skeletal muscle*. *J Appl Physiol*, 1981. **50**(6): p. 1272-6.
135. Dunn, S.E., J.L. Burns, and R.N. Michel, *Calcineurin is required for skeletal muscle hypertrophy*. *J Biol Chem*, 1999. **274**(31): p. 21908-12.
136. Dunn, S.E. and R.N. Michel, *Coordinated expression of myosin heavy chain isoforms and metabolic enzymes within overloaded rat muscle fibers*. *Am J Physiol*, 1997. **273**(2 Pt 1): p. C371-83.
137. Girgenrath, S., K. Song, and L.A. Whittemore, *Loss of myostatin expression alters fiber-type distribution and expression of myosin heavy chain isoforms in slow- and fast-type skeletal muscle*. *Muscle Nerve*, 2005. **31**(1): p. 34-40.
138. Lovering, R.M., A.B. McMillan, and R.P. Gullapalli, *Location of myofiber damage in skeletal muscle after lengthening contractions*. *Muscle & Nerve*, 2009. **40**(4): p. 589-594.
139. Hasselman, C.T., T.M. Best, A.V. Seaber, and W.E. Garrett, *A Threshold and Continuum of Injury During Active Stretch of Rabbit Skeletal Muscle*. *The American Journal of Sports Medicine*, 1995. **23**(1): p. 65-73.
140. Tetsuro, T., A. Akira, T. Masayoshi, U. Shuichi, and S. Takemasa, *Characteristics of compensatory hypertrophied muscle in the rat: I. Electron microscopic and immunohistochemical studies*. *The Anatomical Record*, 1996. **246**(3): p. 325-334.
141. Karalaki, M., S. Fili, A. Philippou, and M. Koutsilieris, *Muscle Regeneration: Cellular and Molecular Events*. *In Vivo*, 2009. **23**(5): p. 779-796.
142. Karalaki, M., S. Fili, A. Philippou, and M. Koutsilieris, *Muscle regeneration: cellular and molecular events*. *In Vivo*, 2009. **23**(5): p. 779-96.
143. Mantilla, C.B., R.V. Sill, B. Aravamudan, W.Z. Zhan, and G.C. Sieck, *Developmental effects on myonuclear domain size of rat diaphragm fibers*. *J Appl Physiol*, 2008. **104**(3): p. 787-94.

144. Allouh, M.Z., Z. Yablonka-Reuveni, and B.W.C. Rosser, *Pax7 Reveals a Greater Frequency and Concentration of Satellite Cells at the Ends of Growing Skeletal Muscle Fibers*. *J. Histochem. Cytochem.*, 2008. **56**(1): p. 77-87.
145. Deng, C., X. Yu, S. Kuang, W. Zhang, Z. Zhou, K. Zhang, W. Qian, Z. Shan, M. Yang, S. Wu, and S. Lin, *Effects of carvedilol on transient outward and ultra-rapid delayed rectifier potassium currents in human atrial myocytes*. *Life Sci*, 2007. **80**(7): p. 665-71.
146. Hei, M.Y., M.L. Xiao, and S.J. Kuang, [*Expression of phosphorylated NMDA receptor 1 in the cerebral cortex after NMDA microinjection in vivo*]. *Zhongguo Dang Dai Er Ke Za Zhi*, 2007. **9**(1): p. 51-3.
147. Kuang, S., K. Kuroda, F. Le Grand, and M.A. Rudnicki, *Asymmetric self-renewal and commitment of satellite stem cells in muscle*. *Cell*, 2007. **129**(5): p. 999-1010.
148. Montarras, D., C. Lindon, C. Pinset, and P. Domyne, *Cultured myf5 null and myoD null muscle precursor cells display distinct growth defects*. *Biol Cell*, 2000. **92**(8-9): p. 565-72.
149. Bischoff, R. and C. Heintz, *Enhancement of skeletal muscle regeneration*. *Dev Dyn*, 1994. **201**(1): p. 41-54.
150. Collins, C.A., I. Olsen, P.S. Zammit, L. Heslop, A. Petrie, T.A. Partridge, and J.E. Morgan, *Stem cell function, self-renewal, and behavioral heterogeneity of cells from the adult muscle satellite cell niche*. *Cell*, 2005. **122**(2): p. 289-301.
151. Hyatt, J.P., G.E. McCall, E.M. Kander, H. Zhong, R.R. Roy, and K.A. Huey, *PAX3/7 expression coincides with MyoD during chronic skeletal muscle overload*. *Muscle Nerve*, 2008. **38**(1): p. 861-6.
152. Bischoff, R. and H. Holtzer, *Inhibition of myoblast fusion after one round of DNA synthesis in 5'-bromodeoxyuridine*. *J. Cell Biol.*, 1970. **44**(1): p. 134-150.
153. Matsuda, R., A. Nishikawa, and H. Tanaka, *Visualization of Dystrophic Muscle Fibers in Mdx Mouse by Vital Staining with Evans Blue: Evidence of Apoptosis in Dystrophin-Deficient Muscle*. *J Biochem*, 1995. **118**(5): p. 959-963.
154. Amthor, H., R. Macharia, R. Navarrete, M. Schuelke, S.C. Brown, A. Otto, T. Voit, F. Muntoni, G. Vrbóva, T. Partridge, P. Zammit, L. Bünger, and K. Patel, *Lack of myostatin results in excessive muscle growth but impaired force generation*. *Proceedings of the National Academy of Sciences*, 2007. **104**(6): p. 1835-1840.
155. Lee, S.-J., *Quadrupling Muscle Mass in Mice by Targeting TGF- β Signaling Pathways*. *PLoS ONE*, 2007. **2**(8): p. e789.
156. Girgenrath, S., K. Song, and L.A. Whittemore, *Loss of myostatin expression alters fiber-type distribution and expression of myosin heavy chain isoforms in slow- and fast-type skeletal muscle*. *Muscle & Nerve*, 2005. **31**(1): p. 34-40.
157. Allen, D.L. and T.G. Unterman, *Regulation of myostatin expression and myoblast differentiation by FoxO and SMAD transcription factors*. *Am J Physiol Cell Physiol*, 2007. **292**(1): p. C188-99.
158. Hennebry, A., C. Berry, V. Siriatt, P. O'Callaghan, L. Chau, T. Watson, M. Sharma, and R. Kambadur, *Myostatin regulates fiber-type composition of skeletal muscle by regulating MEF2 and MyoD gene expression*. *Am J Physiol Cell Physiol*, 2009. **296**(3): p. C525-34.
159. Michel, R.N., E.R. Chin, J.V. Chakkalakal, J.K. Eibl, and B.J. Jasmin, *Ca²⁺/calmodulin-based signalling in the regulation of the muscle fibre phenotype and its therapeutic potential via modulation of utrophin A and myostatin expression*. *Appl Physiol Nutr Metab*, 2007. **32**(5): p. 921-9.
160. Matsakas, A., E. Mouisel, H. Amthor, and K. Patel, *Myostatin knockout mice increase oxidative muscle phenotype as an adaptive response to exercise*. *J Muscle Res Cell Motil*.

161. Li, Z.B., H.D. Kollias, and K.R. Wagner, *Myostatin directly regulates skeletal muscle fibrosis*. J. Biol. Chem., 2008: p. M802585200.
162. Welle, S., A. Cardillo, M. Zanche, and R. Tawil, *Skeletal muscle gene expression after myostatin knockout in mature mice*. Physiol. Genomics, 2009. **38**(3): p. 342-350.
163. Mendias, C.L., K.I. Bakhurin, and J.A. Faulkner, *Tendons of myostatin-deficient mice are small, brittle, and hypocellular*. Proceedings of the National Academy of Sciences, 2008. **105**(1): p. 388-393.
164. Narici, M.V. and C.N. Maganaris, *Adaptability of elderly human muscles and tendons to increased loading*. Journal of Anatomy, 2006. **208**(4): p. 433-443.
165. Seynnes, O.R., R.M. Erskine, C.N. Maganaris, S. Longo, E.M. Simoneau, J.F. Grosset, and M.V. Narici, *Training-induced changes in structural and mechanical properties of the patellar tendon are related to muscle hypertrophy but not to strength gains*. J Appl Physiol, 2009. **107**(2): p. 523-530.
166. Kubo, K., T. Ikebukuro, H. Yata, N. Tsunoda, and H. Kanehisa, *Time Course of Changes in Muscle and Tendon Properties During Strength Training and Detraining*. The Journal of Strength & Conditioning Research. **24**(2): p. 322-331 10.1519/JSC.0b013e3181c865e2.
167. Wehling, M., B. Cai, and J.G. Tidball, *Modulation of myostatin expression during modified muscle use*. FASEB J., 2000. **14**(1): p. 103-110.
168. Arnold, L., A. Henry, F. Poron, Y. Baba-Amer, N. van Rooijen, A. Plonquet, R.K. Gherardi, and B. Chazaud, *Inflammatory monocytes recruited after skeletal muscle injury switch into antiinflammatory macrophages to support myogenesis*. J. Exp. Med., 2007. **204**(5): p. 1057-1069.
169. McLennan, I.S., *Degenerating and regenerating skeletal muscles contain several subpopulations of macrophages with distinct spatial and temporal distributions*. J Anat, 1996. **188 (Pt 1)**: p. 17-28.
170. Tidball, J.G., *Inflammatory processes in muscle injury and repair*. Am J Physiol Regul Integr Comp Physiol, 2005. **288**(2): p. R345-353.
171. Trappe, T.A., F. White, C.P. Lambert, D. Cesar, M. Hellerstein, and W.J. Evans, *Effect of ibuprofen and acetaminophen on postexercise muscle protein synthesis*. Am J Physiol Endocrinol Metab, 2002. **282**(3): p. E551-556.
172. Bondesen, B.A., S.T. Mills, K.M. Kegley, and G.K. Pavlath, *The COX-2 pathway is essential during early stages of skeletal muscle regeneration*. Am J Physiol Cell Physiol, 2004. **287**(2): p. C475-483.
173. Novak, M.L., W. Billich, S.M. Smith, K.B. Sukhija, T.J. McLoughlin, T.A. Hornberger, and T.J. Koh, *COX-2 inhibitor reduces skeletal muscle hypertrophy in mice*. Am J Physiol Regul Integr Comp Physiol, 2009. **296**(4): p. R1132-1139.
174. Ishido, M., K. Kami, and M. Masuhara, *Localization of MyoD, myogenin and cell cycle regulatory factors in hypertrophying rat skeletal muscles*. Acta Physiologica Scandinavica, 2004. **180**(3): p. 281-289.
175. Sakuma, K., J. Nishikawa, R. Nakao, H. Nakano, M. Sano, and M. Yasuhara, *Serum response factor plays an important role in the mechanically overloaded plantaris muscle of rats*. Histochemistry and Cell Biology, 2003. **119**(2): p. 149-160.
176. Ishido, M., M. Uda, N. Kasuga, and M. Masuhara, *The expression patterns of Pax7 in satellite cells during overload-induced rat adult skeletal muscle hypertrophy*. Acta Physiologica, 2009. **195**(4): p. 459-469.
177. Sicinski, P., Y. Geng, A.S. Ryder-Cook, E.A. Barnard, M.G. Darlison, and P.J. Barnard, *The molecular basis of muscular dystrophy in the mdx mouse: a point mutation*. Science, 1989. **244**(4912): p. 1578-1580.

178. Jejurikar, S.S. and W.M. Kuzon, *Satellite cell depletion in degenerative skeletal muscle. Apoptosis*, 2003. **8**(6): p. 573-578.
179. Wagner, K.R., A.C. McPherron, N. Winik, and S.J. Lee, *Loss of myostatin attenuates severity of muscular dystrophy in mdx mice. Annals of Neurology*, 2002. **52**(6): p. 832-836.
180. Gilson, H., O. Schakman, S. Kalista, P. Lause, K. Tsuchida, and J.-P. Thissen, *Follistatin induces muscle hypertrophy through satellite cell proliferation and inhibition of both myostatin and activin. Am J Physiol Endocrinol Metab*, 2009. **297**(1): p. E157-164.
181. Rosenblatt, J.D. and D.J. Parry, *Gamma irradiation prevents compensatory hypertrophy of overloaded mouse extensor digitorum longus muscle. J Appl Physiol*, 1992. **73**(6): p. 2538-2543.
182. Armstrong, D.D., V.L. Wong, and K.A. Esser, *Expression of beta-catenin is necessary for physiological growth of adult skeletal muscle. Am J Physiol Cell Physiol*, 2006. **291**(1): p. C185-188.
183. Matheny, R.W., E. Merritt, S.V. Zannikos, R.P. Farrar, and M.L. Adamo, *Serum IGF-I deficiency does not prevent compensatory skeletal muscle hypertrophy in resistance exercise. Proc Soc Exp Biol Med*, 2008: p. 0808-RM-251.
184. Peng, Z., C. Xiaoping, and F. Ming, *Signaling mechanisms involved in disuse muscle atrophy. Medical hypotheses*, 2007. **69**(2): p. 310-321.
185. Muller, F.L., W. Song, Y.C. Jang, Y. Liu, M. Sabia, A. Richardson, and H. Van Remmen, *Denervation-induced skeletal muscle atrophy is associated with increased mitochondrial ROS production. Am J Physiol Regul Integr Comp Physiol*, 2007. **293**(3): p. R1159-1168.
186. Sharma, M., R. Kambadur, K.G. Matthews, W.G. Somers, G.P. Devlin, J.V. Conaglen, P.J. Fowke, and J.J. Bass, *Myostatin, a transforming growth factor- β ; superfamily member, is expressed in heart muscle and is upregulated in cardiomyocytes after infarct. Journal of Cellular Physiology*, 1999. **180**(1): p. 1-9.
187. Gilson, H., O. Schakman, L. Combaret, P. Lause, L. Grobet, D. Attaix, J.M. Ketelslegers, and J.P. Thissen, *Myostatin Gene Deletion Prevents Glucocorticoid-Induced Muscle Atrophy. Endocrinology*, 2007. **148**(1): p. 452-460.
188. McMahon, C.D., L. Popovic, J.M. Oldham, F. Jeanplong, H.K. Smith, R. Kambadur, M. Sharma, L. Maxwell, and J.J. Bass, *Myostatin-deficient mice lose more skeletal muscle mass than wild-type controls during hindlimb suspension. Am J Physiol Endocrinol Metab*, 2003. **285**(1): p. E82-87.
189. Michel, R.N., R.J. Campbell, and B.J. Jasmin, *Regulation of succinate dehydrogenase within muscle fiber compartments by nerve-mediated activity and CNTF. Am J Physiol Regul Integr Comp Physiol*, 1996. **270**(1): p. R80-85.
190. Tsika, R.W., R.E. Herrick, and K.M. Baldwin, *Time course adaptations in rat skeletal muscle isomyosins during compensatory growth and regression. J Appl Physiol*, 1987. **63**(5): p. 2111-2121.
191. Heineke, J., M. Auger-Messier, J. Xu, M. Sargent, A. York, S. Welle, and J.D. Molkentin, *Genetic Deletion of Myostatin From the Heart Prevents Skeletal Muscle Atrophy in Heart Failure. Circulation*. **121**(3): p. 419-425.
192. Bish, L.T., K.J. Morine, M.M. Sleeper, and H.L. Sweeney, *Myostatin Is Upregulated Following Stress in an Erk-Dependent Manner and Negatively Regulates Cardiomyocyte Growth in Culture and in a Mouse Model. PLoS ONE*, 2010. **5**(4): p. e10230.
193. Cameron, V.A., E. Nishimura, L.S. Mathews, K.A. Lewis, P.E. Sawchenko, and W.W. Vale, *Hybridization histochemical localization of activin receptor subtypes in rat brain, pituitary, ovary, and testis. Endocrinology*, 1994. **134**(2): p. 799-808.

194. Allen, D.L., A.S. Cleary, K.J. Speaker, S.F. Lindsay, J. Uyenishi, J.M. Reed, M.C. Madden, and R.S. Mehan, *Myostatin, activin receptor 11b, and follistatin-like-3 gene expression are altered in adipose tissue and skeletal muscle of obese mice*. *Am J Physiol Endocrinol Metab*, 2008. **294**(5): p. E918-927.
195. Gu, Z., L.M. Steinmetz, X. Gu, C. Scharfe, R.W. Davis, and W.-H. Li, *Role of duplicate genes in genetic robustness against null mutations*. *Nature*, 2003. **421**(6918): p. 63-66.

Appendix A: Summary of values used for overload

Non- OV	CSA										Proportions (%)				
	Midbelly	Major I	Major IIa	Major IIx	Major IIb	Total CSA	Est. Cell count	MW (mg)	R MW (mg/g)	Major I	Major IIa	Major IIx	Major IIb		
WT															
F67-5	1700053	832.4	1008.6	1585.6	2418.4	1586.5	1069.4	22.0	67.2	4.78	45.22	53.42	28.07		
G54-5	1448761		777.8	1167.1	1987.4	1558.5	929.6	21.0	57.7	0.00	21.94	36.72	58.53		
C57stock	1649659	1032.7	1089.7	1415.2	2424.0	1745.7	945.6	18.2	70.8	0.28	40.69	34.32	42.05		
E68-3	1677341	582.0	1043.2	1554.2	2379.0	1613.1	1039.9	24.2	85.9	0.32	46.53	44.52	33.47		
KO															
J92-1	2667716		1120.7	1440.5	2605.0	2091.7	1275.1	36.6	105.3	0.00	21.04	42.65	59.78		
J91-4	2932506		812.4	1266.5	2658.2	1985.5	1476.8	42.6	103.7	0.00	22.42	45.90	56.37		
J90-2	2545629		1369.7	2051.7	2612.0	2205.7	1154.1	30.7	107.5	0.00	25.29	33.24	52.81		
J118-4	2690442		932.5	1627.0	2814.8	2211.9	1216.4	40.6	106.8	0.00	21.34	43.64	61.84		
3day OV															
WT															
E65-1	1822437	1114.0	1112.4	1501.1	2037.4	1507.5	1208.9	20.7	89.4	7.04	41.51	36.50	34.29		
F74-1	2553059	972.1	960.1	1538.2	2569.4	1751.6	1457.6	30.6	91.2	0.41	37.65	38.63	42.12		
G56-4	1564436	849.2	889.7	1469.7	2065.7	1358.4	1152.5	27.1	86.9	1.02	46.75	37.98	30.97		
C57STK	1315450	593.0	865.4	1410.2	2020.9	1371.7	959.0	16.1	56.3	0.77	42.33	41.56	31.46		
KO															
J104-1	4779264		1236.4	1704.4	2427.1	2023.5	2361.9	33.25	94.2	0.00	20.44	46.63	55.21		
J107-1	38777w36		1233.6	1663.3	2336.1	1911.5	2028.6	30.65	114.4	0.00	34.53	35.16	51.75		
J105-2	3512238		929.5	1785.3	3043.2	2377.9	1477.1	30.7	99.7	0.00	22.15	19.98	62.94		
J111-1	3689021		1073.7	1615.9	2161.0	1781.2	2071.1	46.0	130.7	0.00	29.92	29.34	50.65		

Appendix A (cont'd)

2week OV	CSA											Proportions (%)				
	Animal	Midbelly	Major I	Major IIa	Major IIx	Major IIb	Total CSA	Est. Cell count	MW (mg)	R MW (mg/g)	Major I	Major IIa	Major IIx	Major IIb		
WT	C57stk	2580354	1548.9	1869.5	2266.6	2849.2	2289.8	1126.1	55.8	174.2	0.79	39.71	49.94	36.03		
	F70-2	1977533	1199.8	1393.5	2021.7	2219.3	1718.0	1150.3	26.6	109.3	11.45	51.79	39.24	20.79		
	G64-1	1998368		1275.5	1912.2	2372.2	1728.9	1157.9	37.6	135.6	0.00	50.74	38.39	33.46		
	G66-3	2308537	882.5	1259.7	2198.2	2880.1	1996.9	1150.5	34.4	118.9	7.42	39.36	52.75	35.28		
	W8-4	1725250	1122.3	1410.8	2217.8	2801.9	1857.4	926.6	39.8	132.7	7.52	54.91	45.05	22.46		
KO	J95-1	3211185		1484.6	2082.5	2774.1	2336.5	1375.9	49.6	169.7	0.00	21.25	47.38	58.86		
	J95-2	3161743	1099.6	1184.2	1584.9	2242.4	1869.6	1684.9	51.9	140.3	0.63	25.06	37.70	62.74		
	J121-2	2699168		945.9	1384.6	2373.6	1847.3	1461.2	37.7	110.1	0.00	23.18	31.71	56.56		
	J127-3	3545387		1236.4	1747.0	2343.0	2014.6	1755.1	48.8	127.4	0.00	23.65	47.41	57.47		
6week OV	B122-1	2348038	1488.4	1958.8	2878.2	3887.0	2586.8	907.7	37.2	111.0	15.30	34.19	49.13	19.66		
	E55-1	3750789	1851.1	1947.1	2726.7	3095.2	2470.7	1518.1	49.6	167.4	15.63	43.53	30.40	28.53		
	Jack2	3129009	1421.7	1553.5	2151.7	2598.7	1966.0	1589.7	40.0	129.0	7.66	47.00	44.40	25.66		
	Jack4	3542195	1473.5	1719.3	2535.9	3172.8	2375.3	1489.1	45.5	157.4	12.18	38.97	42.83	29.45		
	Jack5	3580272	1081.1	1617.4	2097.3	2368.9	1830.5	1954.1	44.9	162.7	10.10	53.14	45.61	18.64		
W3-3	2060449	1301.6	1661.2	2264.4	2839.1	1944.3	1059.7	46.0	177.6	10.63	62.21	45.51	14.26			
KO	J85-1	3019782		1480.5	2054.3	2598.4	2203.2	1370.6	45.5	140.0	0.00	27.37	51.23	52.21		
	J85-3	3632605		1504.8	2224.4	2963.0	2416.5	1503.2	64.3	193.5	0.00	26.52	47.98	52.97		
	J110-1	2901172		1357.7	1824.9	2542.3	2040.2	1422.0	57.6	140.5	0.00	33.83	58.44	44.71		
	J126-2	2744543	1268.9	1270.7	2564.0	2982.7	2332.5	1176.7	54.2	137.2	1.00	30.33	43.67	56.06		
	J127-1	2375637	1071.1	1432.0	2286.5	2897.6	2222.4	1068.9	47.0	155.0	3.57	36.49	53.49	35.03		

**Appendix B: Summary of values used for denervation:
Soleus muscle**

WT N-DEN	CSA										Proportions				
	Midbelly	Major I	Major Ila	Major Ilix	Major Ilib	Total CSA	Abs MW	REL MW	Major I	Major Ila	Major Ilix	Major Ilib			
F67-5	1344440	1212.8	1374.5	2030.7	2420.4	1409.7	11.0	33.6	28.3	41.4	37.1	11.3			
	1477371	1432.8	1489.7	2019.6	1389.3	1560.6	10.8	33.0	42.2	49.5	15.6	5.7			
G54-5	1566780	1817.6	1544.8	1774.7	2345.5	1737.3	10.0	27.5	54.3	42.0	17.3	2.3			
	1467725	1690.0	1619.7	1773.3	1622.4	1656.6	10.4	28.7	47.9	48.7	8.3	2.8			
C57stock	1131340	1609.2	1233.9	990.4		1425.9	11.3	44.0	52.0	44.4	7.2	0.0			
	1226075	1763.3	1288.3	1327.7	1151.4	1541.1	10.9	42.4	53.5	45.1	3.7	0.6			
KO N-DEN															
J92-1	1887897	1670.8	1737.9	2130.2		1760.9	17	48.2	45.1	45.2	14.2	0.0			
	1506722	1703.8	1517.1	1893.1	1755.5	1647.7	16.8	47.6	30.0	54.2	16.9	4.8			
J91-4	2146799	2103.4	1986.2	2412.5	2694.0	2120.2	16.5	40.8	40.7	49.5	19.7	4.7			
	2227234	1962.2	1782.4	1777.0	2261.3	1931.2	17.5	43.3	47.6	45.3	8.6	10.3			
J90-2	1835676	2162.7	1664.3	2098.7		1948.17	13.3	46.7	50.9	45.9	10.2	0.0			
	2157480	2051.8	1758.3	2386.7	2254.8	1966.1	13.5	47.4	41.2	48.4	15.1	0.7			

Appendix B (cont'd)

WT DEN	Midbelly	CSA						Abs MW	REL MW	Proportions			
		Major I	Major IIa	Major IIx	Major IIb	Total CSA	Major I			Major IIa	Major IIx	Major IIb	
E57-2	N-DEN	1594923	2080.9	1756.0	1929.4	1919.1	11.2	38.9	44.6	49.8	13.6	0.0	
	DEN	989174.8	1626.0	1169.7	1265.1	1341.4	9.1	31.6	35.2	53.9	12.8	4.9	
G53-1	N-DEN	1036544	1949.3	1649.9	1815.2	1853.2	9	29.5	60.3	37.4	9.2	3.7	
	DEN	641096.7	551.8	696.7	777.2	642.2	5	16.4	43.8	52.1	17.9	0.0	
F72-1	N-DEN		1350.8	1344.6	1654.2	1379.4	10.2	29.3	43.3	58.2	15.2	0.0	
	DEN		716.3	834.4	1213.5	921.7	6.7	19.3	24.5	70.1	30.3	0.0	
E56-2	N-DEN	1072487	1949.7	1558.1	1577.2	1739.0	9	39.1	46.6	40.7	19.8	1.4	
	DEN	546086	1401.1	1041.8	1199.1	1211.9	6.5	28.3	48.5	49.8	5.7	0.0	
KO DEN													
J91-1	N-DEN	2333954	2443.2	2040.7	2496.9	2445.1	15	44.4	28.3	41.4	37.1	11.3	
	DEN	1202005	1383.9	1201.7	1448.3	1316.2	9.7	28.7	42.2	49.5	15.6	5.7	
J91-2	N-DEN	2930884	2857.5	2602.2	2866.3	2849.2	15.7	41.4	43.6	56.1	32.6	6.5	
	DEN	1228565	1432.1	1259.5	1416.2	1355.1	8.9	23.5	42.0	54.4	21.5	1.3	
J101-1	N-DEN	2930884	2090.7	1953.6	2574.4	2109.9	14.6	39.5	20.1	68.7	22.1	4.1	
	DEN	1228565	1586.7	1303.5	1438.4	1420.203	9.5	25.7	30.9	57.8	17.2	8.5	
J90-3	N-DEN	1885462	1921.3	1710.4	2125.2	1883.008	16.1	54.4	49.1	39.1	16.6	4.3	
	DEN	789573.2	1411.7	899.9	1227.6	1230.737	10	38.8	63.0	34.6	6.3	0.0	

**Appendix C: Summary of values used for denervation:
Plantaris muscle**

WT N-DEN	CSA										Proportions				
	Midbelly	Major I	Major IIa	Major IIx	Major IIb	Total CSA	Abs MW	REL MW	Major I	Major IIa	Major IIx	Major IIb			
F67-5	1496851	680.1	988.9	1566.7	2301.8	1549.6	21.5	65.7	5.46	40.56	45.87	31.17			
	1565533	984.7	1028.2	1604.5	2534.9	1623.4	22.5	68.8	4.09	49.88	60.96	24.96			
G54-5	1240219		777.8	1167.1	1987.4	1558.5	20.1	55.4	0.00	21.94	36.72	58.53			
	951084.5	737.9	682.7	1210.0	1922.5	1396.8	21.8	60.1	2.15	27.40	34.17	47.25			
C57stock	1349514		961.7	1289.8	2371.4	1697.8	18.3	71.2	0.00	40.09	30.33	44.46			
	1498366	1032.7	1217.8	1540.6	2476.7	1793.5	18.1	70.4	0.56	41.30	38.31	39.65			
KO N-DEN															
J92-1	2764984		1054.8	1539.7	2556.4	2107.5	38.5	109.1	0.00	17.32	41.48	63.36			
	2465012		1186.6	1341.3	2653.7	2075.9	34.7	98.3	0.00	24.76	43.81	56.19			
J91-4	2912101		904.2	1414.6	2618.9	2004.7	43.2	106.9	0.00	24.83	47.51	56.50			
	2802026		720.6	1118.4	2697.5	1966.3	41.9	103.7	0.00	20.01	44.28	56.23			
J90-2	2458449		1456.2	1837.3	2706.9	2240.9	30.1	105.6	0.00	27.60	33.61	55.38			
	2545088	1610.3	1283.2	2266.2	2517.2	2170.5	31.2	109.5	0.63	22.99	32.86	50.24			

Appendix C (cont'd)

WT DEN	CSA										Proportions			
	Midbelly	Major I	Major IIa	Major IIx	Major IIb	Total CSA	Abs MW	REL MW	Major I	Major IIa	Major IIx	Major IIb		
E57-2	N-DEN	1998876		1366.8	1904.8	2908.3	2100.8	21.5	74.7	0.00	41.06	57.88	37.63	
	DEN	1178803	1009.3	987.7	1190.6	1554.4	1307.3	15.5	53.8	1.04	29.44	40.26	45.05	
G53-1	N-DEN	1924850	1143.8	958.5	1508.8	2523.6	1804.1	18.7	61.3	1.09	31.94	24.41	48.14	
	DEN	947658.7	743.5	968.6	1179.9	1326.3	1195.3	13.5	44.3	0.35	29.02	35.87	54.20	
F72-1	N-DEN	1924850		1123.6	1891.5	2526.1	1815.5	22.7	65.2	0.00	43.68	41.32	35.00	
	DEN	947658.7		978.5	1524.5	1860.0	1361.7	18.8	54.0	0.00	46.57	38.83	27.32	
E56-2	N-DEN	1541821	922.8	825.7	1300.4	2247.1	1502.6	16.2	70.4	1.28	30.67	35.75	40.60	
	DEN	962798.3		994.6	1377.0	1624.4	1309.2	13.0	56.5	0.00	44.07	38.78	34.57	
KO DEN														
J91-1	N-DEN	2258881	1235.4	1482.3	2037.5	2808.3	2497.8	36.0	106.5	1.04	20.77	36.19	63.09	
	DEN	2087118		1087.1	1497.9	2277.3	1909.4	22.3	66.0	0.00	23.33	36.14	61.29	
J91-2	N-DEN	3104293		919.6	1341.7	2569.4	2221.5	40.0	105.5	0.00	10.54	27.15	76.31	
	DEN	2112363		1029.7	1709.4	2151.3	1839.5	25.8	68.1	0.00	28.56	43.44	53.52	
J101-1	N-DEN	3104293		1275.1	1725.9	3094.7	2360.8	31.6	85.4	0.00	28.23	33.27	55.33	
	DEN	2112363		1318.2	1709.1	2059.7	1771.9	24.8	67.0	0.00	33.51	38.41	50.32	
J90-3	N-DEN	2396218		1172.9	1856.7	2472.8	2097.6	31.0	104.7	0.00	20.16	37.21	60.34	
	DEN	1522493		1220.3	1540.2	1752.9	1579.8	25.8	87.2	0.00	28.56	36.83	58.16	